# Aspartate 120 of *Escherichia coli* Methylenetetrahydrofolate Reductase: Evidence for Major Roles in Folate Binding and Catalysis and a Minor Role in Flavin Reactivity[†,‡]

Elizabeth E. Trimmer,*[,§] David P. Ballou,[||] Lara J. Galloway,[§] Sara A. Scannell,[§] Danielle R. Brinker,[§] and Katie R. Casas[§]

*Department of Chemistry, Grinnell College, Grinnell, Iowa 50112-2036, and Department of Biological Chemistry and Biophysics Research Division, The University of Michigan, Ann Arbor, Michigan 48109-1055*

*Received October 25, 2004; Revised Manuscript Received February 5, 2005*

ABSTRACT: *Escherichia coli* methylenetetrahydrofolate reductase (MTHFR) catalyzes the NADH-linked reduction of 5,10-methylenetetrahydrofolate ($CH_2$-$H_4$folate) to 5-methyltetrahydrofolate ($CH_3$-$H_4$folate) using flavin adenine dinucleotide (FAD) as cofactor. MTHFR is unusual among flavin oxidoreductases because it contains a conserved, negatively rather than positively charged amino acid (aspartate 120) near the N1−C2═O position of the flavin. At this location, Asp 120 is expected to influence the redox properties of the enzyme-bound FAD. Modeling of the $CH_3$-$H_4$folate product into the enzyme active site suggests that Asp 120 may also play crucial roles in folate binding and catalysis. We have replaced Asp 120 with Asn, Ser, Ala, Val, and Lys and have characterized the mutant enzymes. Consistent with a loss of negative charge near the flavin, the midpoint potentials of the mutants increased from 17 to 30 mV. A small kinetic effect on the NADH reductive half-reaction was also observed as the mutants exhibited a 1.2−1.5-fold faster reduction rate than the wild-type enzyme. Catalytic efficiency ($k_{cat}/K_m$) in the $CH_2$-$H_4$-folate oxidative half-reaction was decreased significantly (up to 70000-fold) and in a manner generally consistent with the negative charge density of position 120, supporting a major role for Asp 120 in electrostatic stabilization of the putative 5-iminium cation intermediate during catalysis. Asp 120 is also intimately involved in folate binding as increases in the apparent $K_d$ of up to 15-fold were obtained for the mutants. Examining the $E_{red}$ + $CH_2$-$H_4$folate reaction at 4 °C, we obtained, for the first time, evidence for the rapid formation of a reduced enzyme−folate complex with wild-type MTHFR. The more active Asp120Ala mutant, but not the severely impaired Asp120Lys mutant, demonstrated the species, suggesting a connection between the extent of complex formation and catalytic efficiency.

The flavoprotein methylenetetrahydrofolate reductase (MTHFR)[1] catalyzes the reduction of 5,10-methylenetetrahydrofolate ($CH_2$-$H_4$folate) to 5-methyltetrahydrofolate ($CH_3$-$H_4$folate), as shown in eq 1.

$$CH_2\text{-}H_4\text{folate} + NAD(P)H + H^+ \leftrightarrow CH_3\text{-}H_4\text{folate} + NAD(P)^+ \quad (1)$$

The product $CH_3$-$H_4$folate is the methyl donor in the conversion of homocysteine to methionine; mutations in MTHFR cause elevated levels of homocysteine, an established risk factor for cardiovascular disease (reviewed in ref *1*) and for neural-tube defects (*2*).

We study MTHFR from *Escherichia coli* as a model for the catalytic domain of the human enzyme. Sequence identities are 30% within the catalytic domains of *E. coli*, human, and pig MTHFRs, and the chemical mechanisms of these enzymes are quite similar (*3*, *4*) (K. Yamada, D. P. Ballou, and R. G. Matthews, unpublished results). The X-ray structure of *E. coli* MTHFR is available (*5*); the enzyme is an $\alpha_8\beta_8$ barrel that binds FAD with its *si* face exposed for reactions with substrates. Consistent with the structure are kinetic and stereochemical studies of the *E. coli* and pig liver enzymes. MTHFR employs a ping-pong bi-bi kinetic mechanism (*3*, *4*, *6*), in which the enzyme-bound FAD is reduced by NADH in the reductive half-reaction (shown in eq 2) and the reduced FAD is oxidized by $CH_2$-$H_4$folate in the oxidative half-reaction (shown in eq 3) at rates consistent with overall turnover (*3*, *4*).

[†] This work was supported in part by American Chemical Society Petroleum Research Fund Grant 39599-GB4 (E.E.T.), by Howard Hughes Medical Institute Undergraduate Biological Sciences Education Grant 71100-503702 (Grinnell College), and by National Institutes of Health Grants GM11106 and GM64711 (D.P.B.).

[‡] This paper is dedicated to Vincent Massey (1926−2002).

* To whom correspondence should be addressed. E-mail: trimmere@grinnell.edu. Phone: (641) 269-4398. Fax: (641) 269-4285.

[§] Grinnell College.

[||] The University of Michigan.

[1] Abbreviations: $CH_2$-$H_4$folate, 5,10-methylenetetrahydrofolate; $CH_3$-$H_4$folate, 5-methyltetrahydrofolate; EDTA, ethylenediaminetetraacetic acid; $E_m$, midpoint potential; FAD, flavin adenine dinucleotide; IPTG, isopropyl $\beta$-D-thiogalactoside; MTHFR, methylenetetrahydrofolate reductase; OD, optical density; PCA, protocatechuate; PCD, protocatechuate dioxygenase; $R^2$, linear regression coefficient; $H_4$folate, tetrahydrofolate.

10.1021/bi0477236 CCC: $30.25 
Published on Web 04/14/2005

$$E-FAD_{ox} + NAD(P)H \leftrightarrow E-FAD_{red} + NAD(P)^{+} \quad (2)$$

$$E-FAD_{red} + CH_2\text{-}H_4folate \leftrightarrow E-FAD_{ox} + CH_3\text{-}H_4folate \quad (3)$$

Stereochemically, the reductive half-reaction occurs by transfer of the *pro*-4*S* hydrogen of NAD(P)H as a hydride to the N5 atom at the *si* face of the FAD (*7*, *8*). The NAD(P)$^+$ product is then released from the active site. In the oxidative half-reaction (Scheme 1), $CH_2$-$H_4$folate binds to the enzyme on the *si* face of the FAD (*8*). It is proposed that, just prior to or in concert with reduction of $CH_2$-$H_4$folate, acid-catalyzed opening of the five-membered imidazolidine ring generates a 5-iminium cation intermediate. Transfer of a hydride from N5 of the reduced FAD to the exocyclic methylene (C11) then produces $CH_3$-$H_4$folate (*8*).

Scheme 1: Proposed Mechanism for the Oxidative Half-Reaction

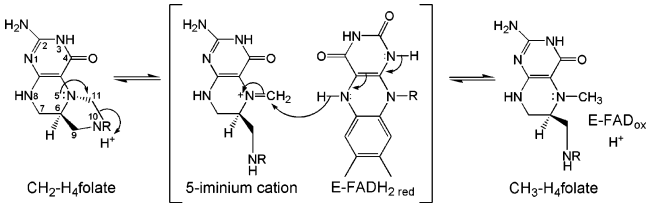


The structure of *E. coli* MTHFR (*5*) has revealed an invariant aspartic acid residue (Asp 120) within 3.8 Å of the N1−C2═O position of the flavin isoalloxazine ring. If Asp 120 is ionized as the carboxylate (p$K_a$ ∼ 4), it would be, to our knowledge, the first case of a negative charge at the N1−C2═O position in the class of flavoproteins that perform dehydrogenation reactions. In the other enzymes in this class, the "N1−C2═O moiety" is a positively charged amino acid (Arg, Lys, or His) or a positive helix dipole (*9*). Three roles for the predominant positive charge at this location have been suggested by previous studies (reviewed in ref *9*). First, by lowering the negative charge density near the flavin, a positive charge would elevate the midpoint potential of the bound flavin, making reduction more thermodynamically favorable. Consistent with this proposal, a Lys266Met mutation in lactate monooxygenase lowered the two-electron midpoint potential by 31 mV (*10*). Second, a positive charge at the N1−C2═O position would likely stabilize preferentially the anionic flavin hydroquinone (Figure 1B) rather than the neutral hydroquinone (Figure 1C) upon reduction. Supporting this view are $^{15}$N NMR experiments (*11*−*13*) and studies examining the stabilization of anionic flavin analogues (*14*). Third, the isolation of inactive, N1−C2═O mutant enzymes devoid of flavin in dihydroorotate dehydrogenase A (Lys164Ala) (*15*) and in trimethylamine dehydrogenase (Arg222Lys) (*16*) suggests a role for a positively charged protein moiety in coenzyme binding. Several studies, however, have been plagued by problems of enzyme inactivity (*15*−*17*), insolubility, and, perhaps, nonspecific structural changes in the flavin environment (*10*).

*E. coli* MTHFR presents an opportunity to study how the unusual, negatively charged Asp 120 at the N1−C2═O position modulates the redox properties of the enzyme-bound FAD. Asp 120 should have the opposite effects on the flavin redox chemistry as a positive charge: (1) lowering the midpoint potential and (2) preferentially stabilizing the neutral flavin hydroquinone (Figure 1C) to prevent unfavorable electrostatic repulsion. We have constructed the following MTHFR variants: Asp120Asn, Asp120Ser, Asp120Ala, Asp120Val, and Asp120Lys. We hypothesize that as the negative charge density of the N1−C2═O moiety decreases, (1) the midpoint potentials of the mutant enzymes will increase, making reduction more facile, and (2) the anionic hydroquinone will be increasingly stabilized at neutral pH. Consistent with hypothesis 1, we have shown, in a previous study, that the neutral Asp120Asn enzyme has a higher midpoint potential than the wild-type enzyme (*18*).

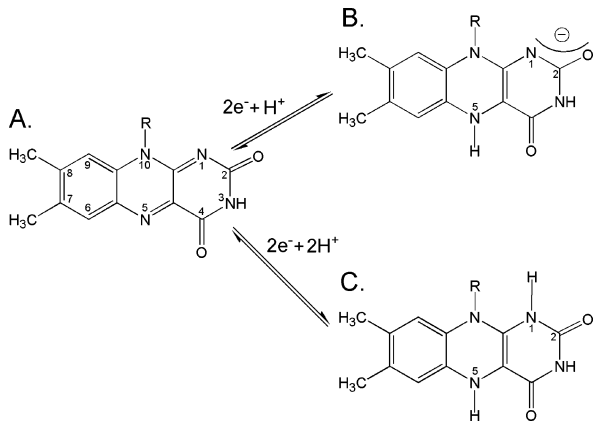


FIGURE 1: Possible structures of oxidized and reduced flavin. (A) Oxidized flavin. (B) Reduced anionic hydroquinone. The negative charge resides at the N1−C2═O position. (C) Reduced neutral hydroquinone, where N1 is protonated. [The p$K_a$ of N1 in solution is 6.7 (*69*).] R refers to ribityl phosphate (FMN) or to ribityl adenylate (FAD).

In the proposed mechanism of reduction of $CH_2$-$H_4$folate by MTHFR, the N10 atom of the substrate is protonated to allow for opening of the imidazolidine ring and generation of a reactive 5-iminium cation intermediate, which then undergoes reduction by hydride transfer (Scheme 1). Although the existence of a 5-iminium cation has not been demonstrated directly in MTHFR, the intermediate is a reasonable first step in activation of the $CH_2$-$H_4$folate for hydride transfer. A similar mechanism of $CH_2$-$H_4$folate activation has been proposed in thymidylate synthase (*19*, *20*), where a 5-$OHCH_2$-$H_4$folate species, the product of the reaction of a 5-iminium cation with water, has been directly observed by X-ray crystallography (*21*).

Modeling of the $CH_3$-$H_4$folate product into the active site of *E. coli* MTHFR (Figure 2) has identified Asp 120 as a residue potentially involved in folate binding and catalysis (*18*). In our model, the pterin ring of $CH_3$-$H_4$folate is stacked against the *si* face of the FAD and the C11 methyl group is situated near N5 of the FAD, a prerequisite for hydride transfer. Two invariant active site residues, Asp 120 and Gln 183, form hydrogen bonds with pterin ring atoms. The recent determination of the structure of an enzyme−$CH_3$-$H_4$folate complex has confirmed the elements of this model (R. Pejchal and M. L. Ludwig, personal communication). On the basis of the structure, two roles for Asp 120 in the mechanism of *E. coli* MTHFR can be envisioned. First, the carboxylate of Asp 120 may aid folate binding through bidentate hydrogen bonding interactions with the N3 and

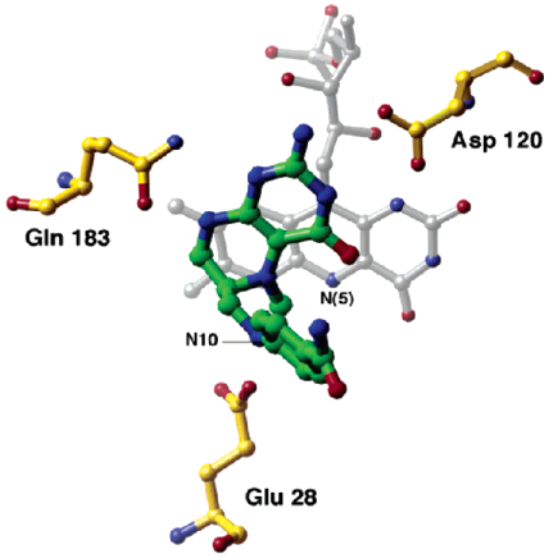


FIGURE 2: Model of $CH_3$-$H_4$folate bound in the active site of *E. coli* methylenetetrahydrofolate reductase. The $CH_3$-$H_4$folate product was generated from 5-formyltetrahydrofolate (folinic acid) (*70*) by removal of the oxygen of the formyl group and repositioning of the pABA ring by rotation of the C6−C9, C9−N10, and N10−pABA bonds. Invariant residues aspartate 120, glutamate 28, and glutamine 183 of MTHFR are shown.

2-amino groups of the pterin ring. Notably, hydrogen bonding between an aspartate and the pterin ring has also been observed in thymidylate synthase (*20*), and in other folate-dependent enzymes (*22*−*30*), although not in serine hydroxymethyltransferase (*31*−*33*). Second, Asp 120 in MTHFR may provide electrostatic stabilization to the putative 5-iminium cation folate intermediate. Although the p$K_a$ of the Asp 120 side chain is not known, the observed increase in midpoint potential for the Asp120Asn mutation (*18*) suggests that Asp 120 exists as the carboxylate anion and could stabilize a developing positive charge on a short-lived 5-iminium cation.

To examine, in a comprehensive manner, the proposed roles for Asp 120 in folate binding and catalysis, we have replaced Asp 120 with amino acids Asn, Ser, Ala, Val, and Lys. In previous work, we found that the apparent affinity of the Asp120Asn mutant for $CH_2$-$H_4$folate is decreased just 2-fold at 25 °C (*18*). This result suggests either that the asparagine retains hydrogen bonding interactions with $CH_2$-$H_4$folate so that it does not impair binding or that Asp 120 is not involved in substrate binding. To distinguish between these proposals, we have prepared the Asp120Ser, -Ala, and -Val mutants, enzymes with a predicted decrease in hydrogen bonding potential compared to that of wild-type MTHFR. A proposed catalytic role for Asp 120 has been supported by a 150-fold decrease in the rate of $CH_2$-$H_4$folate reduction for the Asp120Asn mutant at 25 °C (*18*). If Asp 120 aids catalysis via electrostatic stabilization of the putative 5-iminium cation, catalytic efficiency should decrease according to the negative charge density of the amino acid at position 120.

In this paper, we report the results of investigations of the redox, catalytic, and substrate binding properties of the five MTHFR mutant enzymes: Asp120Asn, Asp120Ser, Asp120Ala, Asp120Val, and Asp120Lys. Our results establish that the invariant Asp 120 is indeed a critical residue for *E. coli* MTHFR, with major roles in folate binding and catalysis, and a minor role in redox modulation. Moreover, by carrying out the rapid-reaction studies at a lower temperature (4 °C) than in our previous work (25 °C) (*4*, *18*), we have demonstrated the formation of pre-steady-state enzyme−folate complexes for the first time and examined their relevance to catalysis.

## EXPERIMENTAL PROCEDURES

*Materials.* NADH, FAD, anthraquinone 2,6-disulfonate, benzyl viologen, xanthine, xanthine oxidase, and protocatechuate (3,4-dihydroxybenzoate) were purchased from Sigma-Aldrich; protocatechuate was recrystallized before being used. Formaldehyde was obtained from Fisher. (6*S*)-$H_4$Folate (sodium salt) was a gift from Merck Eprova AG (Schaffhausen, Switzerland). V. Massey provided 3,10-dimethyl-5-deazaisoalloxazine. Protocatechuate dioxygenase (PCD) was purified from *Pseudomonas cepacia* DB01 (*34*). The Econo-Pac DG-10 columns were purchased from Bio-Rad. Restriction enzymes were purchased from Promega, Vent DNA polymerase and T4 DNA ligase from New England BioLabs, and XL1-Blue competent cells from Stratagene. The λDE3 lysogenization kit was obtained from Novagen (Madison, WI). DNA primers were synthesized by Annovis (Aston, PA) or Sigma Genosys (St. Louis, MO).

Concentrations of the following solutions were determined spectrophotometrically using published extinction coefficients: $\epsilon_{340} = 6230\ M^{-1}\ cm^{-1}$ for NADH (*35*), $\epsilon_{297} = 32\,000\ M^{-1}\ cm^{-1}$ (pH 7.2) for $CH_2$-$H_4$folate (*36*), and $\epsilon_{298} = 28\,400\ M^{-1}\ cm^{-1}$ (pH 7.2) for $H_4$folate (*36*).

*Methods.* All experiments were conducted in 50 mM potassium phosphate (pH 7.2 at 25 °C) containing 0.3 mM EDTA and 10% glycerol (termed protein buffer) at 25 or 4 °C, as noted. UV−vis spectra were recorded with a Shimadzu UV2401PC double-beam spectrophotometer or an Agilent Technologies 8453 diode array spectrophotometer.

*Construction of Asp120 Mutant Plasmids.* The construction of the Asp120Asn plasmid, designated pEET1.8, was described previously (*18*). The Asp120Ser, Asp120Ala, Asp120Val, and Asp120Lys mutant plasmids were constructed using the same procedure, which employs a PCR-based primer overlap extension method (*37*). For each mutation, the pCAS-30 plasmid, which is derived from pET-23b (Novagen) and contains the *E. coli* MTHFR coding sequence juxtaposed with a C-terminal six-histidine tag (*38*), was used as the template for the first round of PCRs. Each mutation was created using a set of two primers, a primer 2* (5′-CTTCCCGGCGGCAGXYZGCCACGCAGCGCC-3′) where the 5′-XYZ-3′ sequences were AGA, CGC, TAC, and TTT for the Asp120Ser, Asp120Ala, Asp120Val, and Asp120Lys mutations, respectively, and a primer 3 (5′-GGCGCTGCGTGGCPDQCTGCCGCCGGGAAG-3′) where the 5′-PDQ-3′ sequences were TCT, GCG, GTA, and AAA, respectively. For all the mutations, primer 1 (5′-gaccacaacg-gtttcccttctagagtcg-3′) and primer 4* (5′-GCTTAAAATCT-TCACCATATCCATGGCAAT-3′) were used to synthesize the outside flanking regions of the gene. The asterisks denote sequences corresponding to the coding strand of the *E. coli* MTHFR gene. Sequences contained within the coding region of the gene are in uppercase letters; those from noncoding regions are in lowercase letters. A *Bss*HII restriction enzyme site was created by the Asp120Ala mutation, while a *Rsa*I

site was created by the Asp120Val mutation. A loss of a *Dpn*I site occurred with each Asp 120 mutation. The sequences of the mutant plasmids were verified by restriction enzyme analyses and by DNA sequencing performed by Sequetech (Mountain View, CA). The mutant plasmids were designated as follows: plasmid pDRB4 contained the Asp120Ser mutation, pEETA3 contained the Asp120Ala mutation, pEETV3 contained the Asp120Val mutation, and pEETK5 contained the Asp120Lys mutation.

*Expression and Purification of Wild-Type and Asp120 Mutant MTHFRs.* Wild-type and Asp120Asn MTHFRs were expressed and purified as described previously (*4*, *18*). The desired strain for producing *E. coli* mutant MTHFR proteins is *E. coli* strain AB1909 (*metF arg lac*) (*39*). This strain contains an uncharacterized mutation in the *E. coli* MTHFR (*metF*) gene, which leads to inactivity of the enzyme and methionine auxotrophy (*39*). Strain AB1909, however, has no source of T7 RNA polymerase, necessary to express the mutant MTHFR genes. The strain was, therefore, lysogenized with $\lambda$DE3 phage, which carry the gene for T7 RNA polymerase under *lacUV5*, to produce strain AB1909(DE3)-7D. This was accomplished using the $\lambda$DE3 lysogenization kit from Novagen and following the procedure provided.

For production of the mutant MTHFRs, strain AB1909-(DE3)7D was transformed with each of the mutant plasmids (pDRB4, pEETA3, pEETV3, and pEETK5). Although polymerase production should be induced by IPTG in these transformed strains, no enhanced production of mutant MTHFR protein was observed upon addition of IPTG, and IPTG was, therefore, not added to any of our cultures. A similar phenomenon was described for the production of wild-type MTHFR in strain BL21(DE3) (*38*). Cells of each freshly transformed, mutant MTHFR strain were inoculated to an $OD_{600}$ of 0.015 in LB medium containing 100 $\mu$g/mL ampicillin and 10 $\mu$M riboflavin. The cells were grown at 37 °C until they reached stationary phase ($OD_{600} \sim 5$), after approximately 12 h. The cells were pelleted, frozen in liquid $N_2$, and stored at −80 °C prior to protein purification. Asp 120 mutant MTHFRs, each containing a C-terminal six-histidine tag, were purified by nickel affinity chromatography as described previously for the Asp120Asn mutant (*18*), except that the purified protein was not concentrated prior to buffer exchange. Typically, 10 mg of purified mutant protein was obtained from 1 L of cell culture.

*Determination of Molar Extinction Coefficients.* The Asp 120 mutant enzymes, diluted to approximately 30 $\mu$M in protein buffer, were denatured to release bound FAD by the addition of an equal volume of 7.5 M guanidine hydrochloride in 1 M Tris-HCl (pH 7.2). For each mutant enzyme, the concentration of liberated FAD at 450 nm was determined as follows. Using the molar extinction coefficient at 450 nm for FAD in aqueous solution at neutral pH, 11 300 $M^{-1}$ $cm^{-1}$ (*40*), the concentration of a solution of free FAD was calculated; upon dilution with guanidine hydrochloride, the molar extinction coefficient of free FAD increased to 11 600 $M^{-1}$ $cm^{-1}$. Using a value of 11 600 $M^{-1}$ $cm^{-1}$ for the extinction coefficient, the absorbance of liberated FAD at 450 nm for each mutant enzyme was converted to concentration. The molar extinction coefficient for each enzyme was then calculated from the $\lambda_{max}$ absorbance of each native protein solution. Throughout this paper, the MTHFR enzyme concentration is expressed as the molarity of enzyme-bound FAD; the enzyme (a tetramer) contains one molecule of FAD per 34 062 Da subunit (*38*).

*Midpoint Potential Determinations*. The midpoint potentials of the Asp 120 mutants were determined spectrophotometrically at pH 7.2 and 25 °C by using the xanthine/xanthine oxidase reducing system with benzyl viologen as the mediator (*41*). The reference redox dye used was anthraquinone 2,6-disulfonate. The $E_m$ for the anthraquinone 2,6-disulfonate redox couple is −184 mV at pH 7.0 (*35*), and at pH 7.2, the $E_m$ is calculated to be −196 mV (*42*). The experiments were performed as described previously (*4*) with minor modifications. The 1.5 mL reaction solution contained 20 $\mu$M enzyme, 42 $\mu$M anthraquinone 2,6-disulfonate, 300 $\mu$M xanthine, 10 $\mu$M benzyl viologen, and 50−60 nM xanthine oxidase in protein buffer. The time-dependent anaerobic reduction of the enzyme and dye was monitored with UV−vis absorbance spectra between 200 and 800 nm. Complete reduction of the system occurred in ∼45 min; turbidity due to precipitation of the enzyme occurred with longer reduction times. Because of overlap between absorbing species, the reduction of neither the dye nor the enzyme could be monitored at a single wavelength. An alternative analysis method, described previously for experiments using the redox dye anthraquinone 1-sulfonate (*18*), was employed. By this method, the concentrations of the oxidized and reduced enzyme or dye were calculated separately from the absorbance at 386 and 474.5 nm from each spectrum, using the following extinction coefficients (E, enzyme; D, dye; all in units of $M^{-1}$ $cm^{-1}$): at 386 nm, $D_{ox}$, 222; $D_{red}$, 7191; $E_{ox}$, 10 858; $E_{red}$, 3993; and at 474.5 nm, $D_{ox}$, 23; $D_{red}$, 1348; $E_{ox}$, 11 802; $E_{red}$, 305. The midpoint potential was determined using the method of Minneart (*43*).

*Stopped-Flow Measurements.* Rapid-reaction studies were carried out in a Hi-Tech Scientific model SF-61 stopped-flow spectrophotometer equipped with a tungsten or deuterium light source for single-wavelength detection or in a Hi-Tech SF-61DX stopped-flow spectrophotometer in single-mixing mode equipped for single-wavelength or diode array detection. For anaerobic work, the instrument was flushed with a 0.1 M potassium phosphate (pH 7) solution containing ∼0.1 unit/mL protocatechuate dioxygenase (PCD) and 200 $\mu$M protocatechuate (PCA, 3,4-dihydroxybenzoate) and allowed to stand overnight (*44*). All measurements were performed at 4 °C in protein buffer (pH 7.2).

The experiments were performed as described previously (*4*) with minor modifications. A solution of enzyme (20 or 100 $\mu$M) and PCD (∼0.1 unit/mL) was placed in a glass tonometer, with PCA in the sidearm, and made anaerobic by 10 cycles of alternate evacuation and equilibration with oxygen-free argon while on ice. The PCA/PCD system was to help maintain anaerobic conditions (*44*). PCA (200 $\mu$M, final concentration) was then introduced from the sidearm. To minimize formation of enzyme turbidity, a glass cup surrounding and attached to the tonometer was filled with ice and used to cool the enzyme solution during the course of the experiment. When reduced enzyme was needed for experiments, 10 mM EDTA and 2 $\mu$M 3,10-dimethyl-5-deazaisoalloxazine were also added to the enzyme solution. Following the gas exchanges and introduction of PCA from the sidearm, the enzyme was photoreduced (*45*) by exposure to visible light from a Sun Gun (Smith Victor Corp., Griffith, IN) while immersed in an ice bath. Control experiments

indicated that the PCD/PCA oxygen-scavenging system had no effect on the measured rate constants.

For experiments involving the NADH substrate, solutions containing various concentrations of NADH and 200 $\mu$M PCA were prepared in protein buffer and bubbled with oxygen-free argon for 10 min. PCD (~0.1 unit/mL, final concentration) was added just prior to use. For experiments involving the (6*R*)-$CH_2$-$H_4$folate substrate, a stock solution (~9 mM) was prepared anaerobically. Solid (6*S*)-$H_4$folate was added to deaerated 50 mM potassium phosphate buffer (pH 8.6) containing 10% glycerol and 0.3 mM EDTA. Following several deoxygenation cycles, formaldehyde (5-fold molar excess) was added. The solution was incubated at room temperature for 30 min to generate (6*R*)-$CH_2$-$H_4$-folate and then placed on ice. The stock solution was kept on ice under a positive pressure of argon for the duration of the experiment. Substrate solutions containing (6*R*)-$CH_2$-$H_4$-folate were prepared by adding various amounts of the stock solution to deaerated protein buffer containing 200 $\mu$M PCA. Formaldehyde was also added, as necessary, to bring the final concentration in all solutions to 1.5 mM (after mixing). PCD (~0.1 unit/mL, final concentration) was added just prior to use. Control experiments performed without added formaldehyde yielded results similar to those obtained with solutions containing 1.5 mM formaldehyde.

Reduction or oxidation of enzyme-bound flavin was followed at 450 nm, that of enzyme−pyridine nucleotide complexes at 550 nm, and that of enzyme−folate complexes at 337 nm. Apparent rate constants were calculated from exponential fits of single-wavelength absorbance traces using one of the following programs that employ the Marquardt−Levenberg algorithm (*46*): KISS (Kinetic Instruments, Inc.), KinetAsyst3 (Hi-Tech Scientific, Salisbury, U.K.), or Program A (developed in the laboratory of D. P. Ballou). Typically, rate constants from three to four shots were averaged, and the error was calculated as the standard deviation. When the values obtained for the observed rate constants demonstrated a hyperbolic dependence on the substrate concentration, the data were fit to eq 4

$$k_{obs} = \frac{k_{max}[S]}{K_d + [S]} \quad (4)$$

where $k_{obs}$ is the observed rate constant, $k_{max}$ is the maximum rate constant at a saturating substrate concentration, [S] is the substrate concentration, and $K_d$ is the apparent dissociation constant for the enzyme−substrate complex, using a nonlinear least-squares fitting algorithm in SigmaPlot (SPSS Inc.).

*NADH−$CH_2$-$H_4$Folate Oxidoreductase Assay.* MTHFR oxidizes NADH and reduces $CH_2$-$H_4$folate to $CH_3$-$H_4$folate in the physiological NADH−$CH_2$-$H_4$folate oxidoreductase assay. The reaction is monitored by the decrease in the NADH absorbance at 340 nm (*47*, *48*) under steady-state kinetic conditions. The assay was performed as described previously (*4*) with minor modifications. All reactions were carried out at 4 °C and pH 7.2 under anaerobic conditions in a Hi-Tech Scientific SF-61 stopped-flow spectrophotometer equipped with a deuterium light source. All samples contained 200 $\mu$M PCA and ~0.1 unit/mL PCD as an oxygen-scavenging system, and formaldehyde was present at a final concentration of 1.5 mM (after mixing). To determine the $K_{mA}$ for NADH, the enzyme (1.25 $\mu$M for the wild type or 2.5 $\mu$M for the Asp 120 mutant, after mixing) was mixed with an equal volume of a solution containing a saturating concentration of (6*R*)-$CH_2$-$H_4$folate (50 $\mu$M for the wild type or 300 $\mu$M for the mutant) and concentrations of NADH varying from 10 to 300 $\mu$M (concentrations after mixing). Similarly, to determine the $K_{mB}$ for $CH_2$-$H_4$folate, enzyme (1.25 $\mu$M for the wild type or 2.5 $\mu$M for the mutant, after mixing) was mixed with an equal volume of solution containing a saturating concentration of NADH (100 $\mu$M) and concentrations of (6*R*)-$CH_2$-$H_4$folate varying from 10 to 600 $\mu$M (concentrations after mixing). All assays were performed in at least triplicate. Initial rates were calculated from the decrease in NADH absorbance at 340 nm over time, using an extinction coefficient of 6230 $M^{-1}$ $cm^{-1}$ for NADH (*35*). All assays were corrected for the initial rate observed when buffer in place of enzyme was mixed with the NADH−$CH_2$-$H_4$folate solutions. The steady-state kinetic parameters for the mutant enzymes were determined by fitting the data to the Michaelis−Menten equation (eq 5).

$$\frac{v}{[E_t]} = \frac{k_{cat}[S]}{K_m + [S]} \quad (5)$$

The wild-type enzyme exhibited substrate inhibition due to both substrates, and the data were fit by successive iterations to eq 6 for double-substrate inhibition in a ping-pong bi-bi system (*49*) using SigmaPlot.

$$\frac{v}{[E_t]} = \frac{[A][B]k_{cat}}{K_{mA}[B](1 + [B]K_{iB}) + K_{mB}[A](1 + [A]/K_{iA}) + [A][B]} \quad (6)$$

## RESULTS

*Spectral Properties of MTHFR Are Modified Slightly by Asp 120 Mutations.* Mutant *E. coli* MTHFRs Asp120Asn, Asp120Ser, Asp120Ala, Asp120Val, and Asp120Lys were expressed in *E. coli* strain AB1909, which carries an uncharacterized mutation in the MTHFR (*metF*) gene leading to enzyme inactivity (*39*). All mutant proteins were produced in soluble form with FAD bound, and as His-tagged proteins, they were purified to homogeneity by employing the same nickel affinity chromatography procedure that was devised for the wild-type enzyme (*4*). The absorbance spectra for the five mutant enzymes are shown in Figure 3. The spectrum of the wild-type enzyme is not shown, but it is identical to that of the Asp120Asn mutant (*4*, *18*). The wavelengths of maximal absorbance for Asp120Ala (445.5 nm) and Asp120Lys (446.0 nm) are red-shifted slightly compared with those of the wild-type, Asp120Asn, and Asp120Ser enzymes (446.5 nm), while that of the Asp120Val mutant (447.5 nm) is blue-shifted slightly. In contrast to the spectra of the wild-type and Asp120Asn enzymes, a small shoulder near 347 nm is prominent in the spectrum of the Asp120Lys mutant and to a lesser extent in the spectra of mutants Asp120Ala, Asp120Ser, and Asp120Val (Figure 3). Molar extinction coefficients, measured at $\lambda_{max}$, were determined to be 14 300 $M^{-1}$ $cm^{-1}$ for each mutant, the same as for the wild-type enzyme (*38*). The mutant enzymes are nonfluorescent, as is

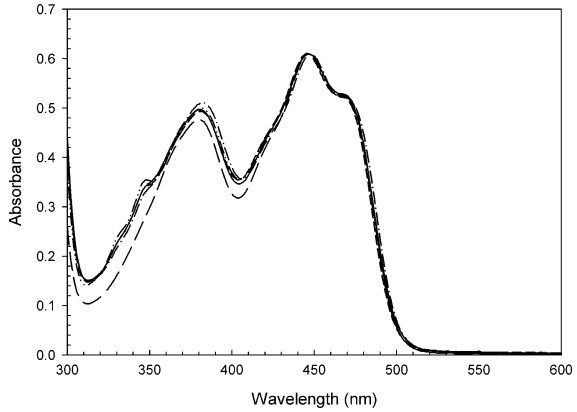


FIGURE 3: UV−visible absorbance spectra of purified Asp 120 mutant MTHFR enzymes. Asp120Asn (− − −), Asp120Ser (—), Asp120Ala (- - -), Asp120Val (-•-), or Asp120Lys (-••-) was diluted to 43 $\mu$M in 50 mM potassium phosphate buffer (pH 7.2) containing 0.3 mM EDTA and 10% glycerol at 25 °C and scanned from 300 to 600 nm. The spectrum of the wild-type enzyme (not shown) is identical to that of the Asp120Asn mutant.

Table 1: Midpoint Potentials[a,b]

| enzyme | $E_m$ (mV) | enzyme | $E_m$ (mV) |
|---|---|---|---|
| wild type | $-237 \pm 4$[c] | Asp120Ala | $-218 \pm 3$ |
| Asp120Asn | $-220 \pm 3$ | Asp120Val | $-214 \pm 3$ |
| Asp120Ser | $-219 \pm 3$ | Asp120Lys | $-207 \pm 3$ |

[a] All measurements were taken at 25 °C in 50 mM potassium phosphate buffer (pH 7.2) containing 0.3 mM EDTA and 10% glycerol. [b] Values are the average of at least three determinations. Uncertainties represent standard deviations. [c] From ref *4*.

the wild-type enzyme (*4*). While the small differences in the spectral properties of the Asp 120 mutants may suggest subtle changes in the environment of the bound FAD, the similarities of the properties to those of the wild-type enzyme suggest that the overall protein structures of the mutants have not been changed significantly. Near-wild-type activity in the reductive half-reaction for each mutant (see below) supports this claim.

*The Midpoint Potential Increases with the Loss of Negative Charge at Position 120.* We have hypothesized that Asp 120 located at the N1−C2═O flavin position will influence the redox properties of MTHFR. A redox dye method developed by Massey (*41*) was used to measure the midpoint potentials of the Asp 120 mutants at 25 °C and pH 7.2. Flavin semiquinone species have not been observed upon photoreduction of the mutants (data not shown); thus, only two-electron midpoint potentials associated with conversion of oxidized to fully reduced hydroquinone were determined. The reference redox dye anthraquinone 2,6-disulfonate with a midpoint potential of −196 mV at pH 7.2 (*42*) was employed. For all the Asp 120 mutants, the resulting log plots were linear (average $R^2 = 0.995 \pm 0.003$) in the region of points corresponding to more than 10% and less than 90% reduced enzyme or dye, and the slopes were near unity (average slope $= 1.19 \pm 0.11$), consistent with the dye and enzyme couples transferring the same number of electrons (presumably two) between the oxidized and reduced forms (*41*).

Table 1 shows the average midpoint potentials determined for the mutants. The midpoint potentials of the variants measured here using anthraquinone 2,6-disulfonate as a redox dye are reasonably similar to potentials measured using the dye anthraquinone 1-sulfonate [$-210 \pm 4$ mV for Asp120Asn (ref *18* and data not shown)]; substantial turbidity, however, plagued measurements of the potentials of some mutants when using anthraquinone 1-sulfonate, but not the 2,6-disulfonate dye. Consistent with the loss of a negatively charged aspartate near the FAD, the measured midpoint potentials of the Asp 120 mutants (Table 1) are higher than that of the wild-type enzyme. Increases in midpoint potential were 17−19 mV (Asp120Asn, -Ser, and -Ala), 23 mV (Asp120Val), and 30 mV (Asp120Lys), which correspond to relative thermodynamic stabilizations of 0.83, 1.1, and 1.4 kcal/mol, respectively, for the reduced enzyme form. Although the observed changes in potential are not large, our results suggest that the amino acid at the N1−C2═O flavin position in *E. coli* MTHFR indeed has the ability to tune the redox properties of the enzyme-bound FAD.

*Reduction by NADH Is Improved by Asp 120 Mutations.* To probe the effect of the five mutations introduced at position 120 on the properties of MTHFR, we examined in detail the reductive and oxidative half-reactions (shown in eqs 2 and 3) constituting the NADH−$CH_2$-$H_4$folate oxidoreductase reaction. To study the reductive half-reaction, the oxidized enzyme (10 $\mu$M) was reacted with concentrations of NADH ranging from 25 to 300 $\mu$M (concentrations after mixing) at pH 7.2 and 4 °C in a stopped-flow spectrophotometer under anaerobic conditions. The 450 nm traces for the Asp120Asn mutant are shown in Figure 4A. The traces were fit to two exponential phases, a fast and a slow phase, accounting for 25 and 75%, respectively, of the total absorbance change. The observed rate constants associated with the slow phase were essentially independent of the concentrations of NADH used in the experiment and reached a maximal value of $20.2 \pm 0.4$ s$^{-1}$ (inset of Figure 4A). In Figure 4A, the decrease in starting absorbance at 450 nm with an increase in NADH concentration may be due to the fast formation of $E_{ox}$•NADH charge-transfer complexes (see below) or, alternately, to surreptitious photochemical reduction of the oxidized enzyme as the experiment progressed.

Transient, weak long-wavelength absorbance, typical of flavin−pyridine nucleotide charge-transfer complexes, was observed for the Asp120Asn enzyme (Figure 4B) at wavelengths between 550 and 650 nm. Such charge-transfer absorbance had been seen for this mutant in our previous studies at 25 °C (*18*), but its kinetic characterization was not possible due to the rate of the reaction at the higher temperature. The 550 nm traces in Figure 4B show two phases, a rapid increase in absorbance followed by a slower decrease. The slow phase data (inset of Figure 4B) yielded a maximal rate constant of $24.8 \pm 0.9$ s$^{-1}$, comparable to the rate of reduction at 450 nm. To estimate the rate constants for formation and decay of the charge-transfer complex, the observed rate constants for the fast phase data at 550 nm were plotted as a function of NADH concentration and fit to a linear function (data not shown). From the slope, the second-order rate constant associated with formation of the complex is estimated to be $(1.5 \pm 0.2) \times 10^6$ M$^{-1}$ s$^{-1}$. From the *y*-intercept, the rate constant for decay of the complex to $E_{ox}$ and NADH is estimated to be $10 \pm 4$ s$^{-1}$, giving an apparent dissociation constant of 7 $\mu$M for the charge-transfer complex of the Asp120Asn enzyme. For comparison, a

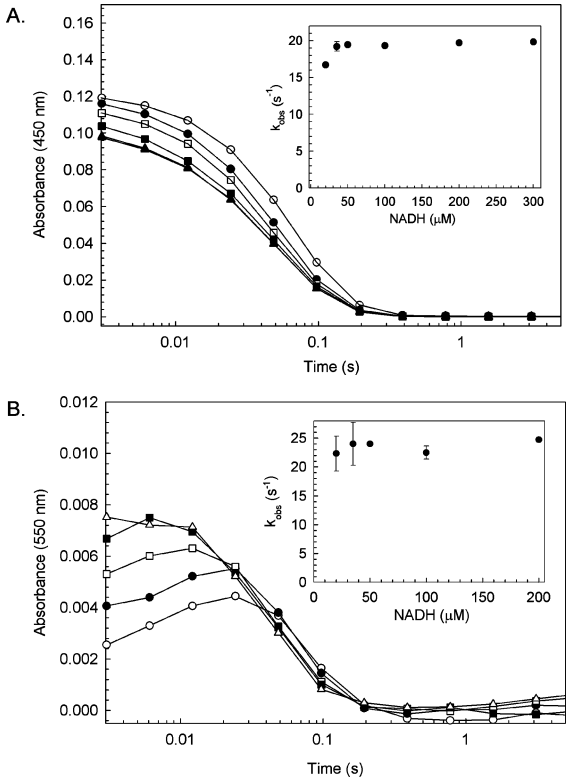


FIGURE 4: Reduction of the Asp120Asn enzyme by NADH. (A) Oxidized enzyme, 10 $\mu$M, was mixed with solutions of 20 (○), 35 (●), 50 (□), 100 (■), 200 (△), and 300 $\mu$M NADH (▲) (concentrations after mixing). Stopped-flow reaction traces, monitored at 450 nm, were fit to two exponential phases. In the inset of panel A, the observed rate constants for reduction (slow phase) were plotted against the concentration of NADH. The maximum rate constant for reduction (net rate constant, $k_2'$, according to Scheme 2) was $20.2 \pm 0.4$ $s^{-1}$. (B) Charge-transfer interactions measured at 550 nm for the reaction of 10 $\mu$M enzyme with 20 (○), 35 (●), 50 (□), 100 (■), and 200 $\mu$M NADH (△) (concentrations after mixing) are shown. In the inset of panel B, the observed rate constants for the slow phase at 550 nm were plotted against the concentration of NADH. The data yielded a maximum rate constant of $24.8 \pm 0.9$ $s^{-1}$. Reaction conditions were 50 mM potassium phosphate buffer (pH 7.2) containing 0.3 mM EDTA and 10% glycerol at 4 °C.

Scheme 2: Kinetic Mechanism for the Reductive Half-Reaction

$$E_{ox} + NADH \underset{k_{-1}}{\overset{k_1}{\rightleftharpoons}} E_{ox}\bullet NADH \overset{CT}{\underset{k_{-2}}{\overset{k_2}{\rightleftharpoons}}} E_{red}\bullet NAD^+ \underset{k_{-3}}{\overset{k_3}{\rightleftharpoons}} E_{red} + NAD^+$$

similar analysis of the wild-type enzyme yielded values of $(6.1 \pm 0.4) \times 10^5$ $M^{-1}$ $s^{-1}$ and $10 \pm 3$ $s^{-1}$ as the second-order and first-order rate constants, respectively, and an apparent dissociation constant of 16 $\mu$M for the charge-transfer complex (data not shown).

Taken together, the results for the Asp120Asn mutant can be described by the minimal kinetic mechanism for the reductive half-reaction, shown as Scheme 2. To test this mechanism, we carried out simulations at both 450 and 550 nm of an A + B ↔ C ↔ D → E + F model for NADH concentrations of 10−200 $\mu$M with the following rate constants: $k_1 = 4 \times 10^6$ $M^{-1}$ $s^{-1}$, $k_{-1} = 30$ $s^{-1}$, $k_2 = 27$ $s^{-1}$, $k_{-2} = 0$ $s^{-1}$, and $k_3 = 100$ $s^{-1}$ (available as Supporting Information). The value used for $k_{-2}$ is zero, consistent with a calculated free energy change for the half-reaction of −4.7 kcal/mol (*4*), making reduction essentially irreversible. These simulations, in which dissociation of NADH from the charge-transfer complex ($k_{-1}$) was on the order of hydride transfer ($k_2$) (not rapid equilibrium) and product release of $NAD^+$ ($k_3$) was comparatively fast (see the Supporting Information), modeled nicely our experimental data at both 450 and 550 nm. At wavelengths between 500 and 800 nm, no transient absorbance consistent with a product $E_{red}$•$NAD^+$ charge-transfer complex was observed, which suggests that $NAD^+$ is released rapidly. The simulated traces at 450 and 550 nm were fit to two exponential phases and the observed rate constants determined. The slow phases showed hyperbolic dependencies on the concentration of NADH and yielded apparent $K_d$ values for NADH of $18 \pm 7$ and $11 \pm 2$ $\mu$M, respectively, for the 450 and 550 nm data (available as Supporting Information). These apparent $K_d$ values obtained from simulation were reasonably similar to the value of 7 $\mu$M that can be calculated from apparent rate constants $k_1$ and $k_{-1}$. From Scheme 2, the net rate constant $k_2'$, equal to the maximal observed rate constant for reduction (slow phase) measured in the stopped-flow spectrophotometer, is given by eq 7 (*50*).

$$k_2' = \frac{k_2 k_3}{k_{-2} + k_3} \tag{7}$$

Stopped-flow analysis as described above for the Asp-120Asn reductive half-reaction was performed, under the same conditions, with wild-type MTHFR and mutants Asp120Ser, Asp120Ala, Asp120Val, and Asp120Lys. Qualitatively, the wild-type and mutant enzymes behaved like the Asp120Asn mutant (Figure 4). For each, the data fit to Scheme 2. Transient charge-transfer absorbance was observed at 550 nm, and the 450 nm traces were biphasic with flavin reduction in the slow phase corresponding to decay of the charge-transfer complex at 550 nm. The slow phase at 450 nm showed no dependence on the NADH concentration, and analyses of the data yielded the respective net rate constants for reduction ($k_2'$) given in Table 2. The results show, within the uncertainty of the measurements, that (1) all mutants catalyze NADH reduction at a somewhat greater rate than the wild-type enzyme and (2) among the mutants, the Asp120Asn mutant is reduced by NADH with the highest $k_2'$.

Table 2: Rapid-Reaction Kinetic Constants for the Reductive Half-Reaction[a,b]

| enzyme | $k_2'$ ($s^{-1}$) | enzyme | $k_2'$ ($s^{-1}$) |
|---|---|---|---|
| wild type | $13.8 \pm 0.4$ | Asp120Ala | $17.6 \pm 0.1$ |
| Asp120Asn | $20.2 \pm 0.4$ | Asp120Val | $17.0 \pm 0.4$ |
| Asp120Ser | $17.6 \pm 0.3$ | Asp120Lys | $17.4 \pm 0.4$ |

[a] All measurements were taken at 4 °C in 50 mM potassium phosphate buffer (pH 7.2) containing 0.3 mM EDTA and 10% glycerol. [b] See Scheme 2 for the definition of rate constants. The net rate constant for reduction, $k_2'$, is defined as $k_2' = k_2k_3/(k_{-2} + k_3)$ (*50*).

*An Intermediate Complex Is Observed in Reaction of the Reduced Wild-Type Enzyme with $CH_2$-$H_4$Folate at 4 °C.* Before the oxidative half-reaction of the Asp 120 mutants could be studied, the reaction of the wild-type enzyme with $CH_2$-$H_4$folate needed to be characterized fully at 4 °C. [The 25 °C temperature used in our previous studies (*4*, *18*) led to substantial turbidity for some of the mutant enzymes.] Photoreduced wild-type enzyme (10 $\mu$M) was combined with

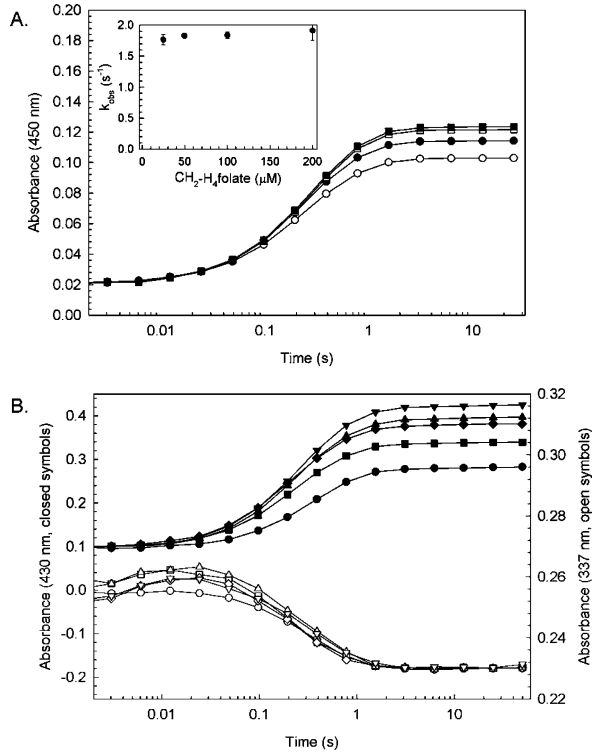


FIGURE 5: Reoxidation of the reduced wild-type enzyme by $CH_2$-$H_4$folate. (A) Photoreduced enzyme (10 $\mu$M) was mixed with solutions of 25 (○), 50 (●), 100 (□), and 200 $\mu$M $CH_2$-$H_4$folate (■) (concentrations after mixing). Stopped-flow reaction traces, monitored at 450 nm, were fit to three exponential phases. The fast, medium, and slow phases accounted for <4, 68, and 28%, respectively, of the total observed absorbance change. In the inset of panel A is shown the dependence of the slow phase on $CH_2$-$H_4$folate concentration. The data yielded a maximal rate constant of 1.9 ± 0.2 $s^{-1}$. (B) Photoreduced enzyme (50 $\mu$M) was mixed with solutions of 25 (○ and ●), 50 (□ and ■), 100 (◇ and ◆), 300 (△ and ▲), and 600 $\mu$M $CH_2$-$H_4$folate (▽ and ▼) (concentrations after mixing). Reaction traces at 430 nm (left axis, filled symbols) and at 337 nm (right axis, empty symbols) are shown. The initial absorbance of the 337 nm traces increased with an increase in substrate concentration due to background absorbance from $CH_2$-$H_4$folate. Thus, the 337 nm traces have been aligned at a beginning absorbance of 0.26 to more easily visualize them. Reaction conditions were 50 mM potassium phosphate buffer (pH 7.2) containing 0.3 mM EDTA and 10% glycerol at 4 °C.

25−200 $\mu$M $CH_2$-$H_4$folate (concentrations after mixing), and the increase in flavin absorbance due to reoxidation was monitored at 450 nm in the stopped-flow apparatus. A representative experiment is shown in Figure 5A. As indicated by spectra recorded at the conclusion of each shot, full reoxidation occurred only at the higher concentrations (100−200 $\mu$M, after mixing) of $CH_2$-$H_4$folate. This reflects the fact that under these conditions the reaction proceeds to equilibrium rather than to completion. [The free energy change of the half reaction is −1.2 kcal/mol (*4*).] In contrast to the reaction studied earlier at 25 °C, which was biphasic (*4*), the 450 nm reaction traces in Figure 5A were best fit to three exponential phases. A fast phase with an estimated rate constant of >200 $s^{-1}$ occurred as an initial lag in the reaction. This phase accounted for less than 4% of the total increase in absorbance (∼0.003 absolute absorbance out of a total change of 0.10). A medium phase, accounting for 68% of the total absorbance change, was independent of the concentration of $CH_2$-$H_4$folate (data not shown) and yielded an observed rate constant of 5.5 ± 0.5 $s^{-1}$. A slow phase, associated with the remaining 28% increase in absorbance, yielded a maximal rate constant of 1.9 ± 0.2 $s^{-1}$ (inset of Figure 5A). The phase appeared to be independent of $CH_2$-$H_4$folate concentration (inset of Figure 5A); by contrast, in our previous study, the corresponding slow phase of reoxidation at 25 °C depended on $CH_2$-$H_4$folate in a hyperbolic manner and yielded an apparent $K_d$ for $CH_2$-$H_4$folate of 11 $\mu$M (*4*).

With the aim of better characterizing the new, fast phase observed at 4 °C, we examined the reaction of a higher concentration of reduced enzyme (50 $\mu$M, 5-fold greater than before) with $CH_2$-$H_4$folate in a stopped-flow spectrophotometer equipped for diode array and single-wavelength detection. Believing that the fast phase might be attributed to the rapid formation of a pre-steady-state enzyme−folate complex, we investigated the reaction at a range of wavelengths from 300 to 800 nm. No changes in absorbance were detected at 550, 650, or 750 nm, wavelengths typical for absorbance of charge-transfer complexes. The reaction monitored at 337 nm, however, suggested the existence of an intermediate species. Figure 5B shows the 337 nm reaction traces (right axis) on the same time scale as the 430 nm traces (left axis). Notably, the absorbance increase at 337 nm corresponds to the lag at 430 nm, and the decrease at 337 nm corresponds to flavin reoxidation at 430 nm. The reaction is triphasic at both wavelengths. The fast phase, characterized by an increase in absorbance at 337 nm, showed no obvious dependence on the concentration of $CH_2$-$H_4$folate, but the uncertainties in the data were large due to the fast rates and small (∼0.03) amplitudes (data not shown). A maximal rate constant of 280 ± 60 $s^{-1}$ was estimated. At 337 nm, the medium and slow phases accounted for 68 and 28%, respectively, of the absorbance decrease, and they exhibited maximal rate constants of 6.0 ± 0.6 and 1.6 ± 0.2 $s^{-1}$, respectively, corresponding to the two phases of reoxidation measured at 430 nm. Our combined results at 337 and 430 nm are consistent with the rapid formation of a reduced enzyme−folate complex followed by its decay, concomitant with reoxidation of the enzyme. This complex could represent an $E_{red}$•$CH_2$-$H_4$folate species, which might be expected to show a perturbation of the reduced enzyme spectrum, or alternatively, the species could be a complex between the reduced enzyme and the putative 5-iminium cation folate intermediate. To test for the existence of the latter, we examined the reaction of reduced enzyme with $CD_2$-$H_4$folate in place of $CH_2$-$H_4$folate in the stopped-flow instrument. If the increase in absorbance at 337 nm were due to the 5-iminium cation in complex with the reduced enzyme, the maximal rate constant associated with the fast phase should exhibit a secondary kinetic isotope effect of 1.3−1.5 (*51*). No such effect, however, was observed (data not shown).

*The $CH_2$-$H_4$Folate Binding Affinity and Rate of Catalysis Are Diminished in the Position 120 Variants*. On the basis of the modeling of $CH_3$-$H_4$folate into the active site of *E. coli* MTHFR (Figure 2), Asp 120 appears to be positioned to participate in folate binding via hydrogen bonding interactions and in folate catalysis through stabilization of the putative 5-iminium cation. Variants Asp120Asn, Asp120Ser, Asp120Ala, Asp120Val, and Asp120Lys, which differ in hydrogen bonding potential and in negative charge density from the wild type, were prepared to test these

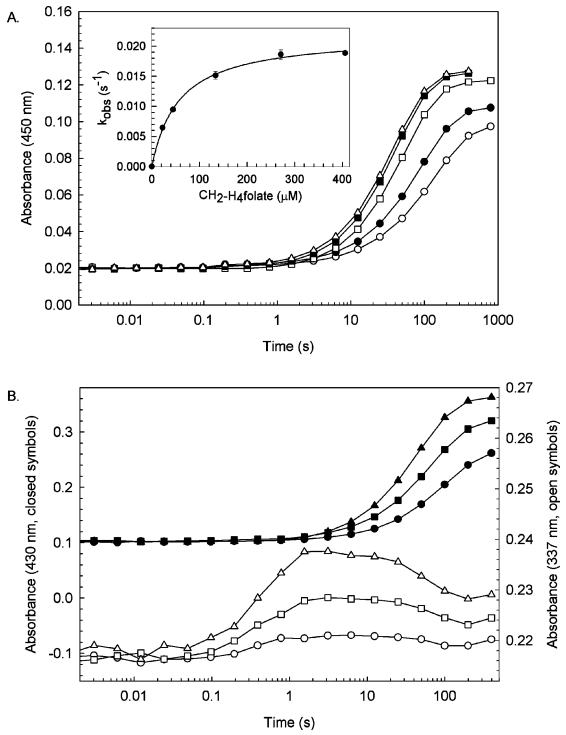


FIGURE 6: Reoxidation of the reduced Asp120Ala enzyme by $CH_2$-$H_4$folate. (A) Photoreduced enzyme (10 $\mu$M) was mixed with solutions of 23 (○), 45 (●), 130 (□), 270 (■), and 410 $\mu$M $CH_2$-$H_4$folate (△) (concentrations after mixing). Stopped-flow reaction traces, monitored at 450 nm, were fit to three exponential phases. The fast, medium, and slow phases accounted for <4, 58, and 38%, respectively, of the total observed absorbance change. In the inset of panel A is shown the dependence of the slow phase on $CH_2$-$H_4$folate concentration. Fit of the data to eq 4 yielded a maximal rate constant of reoxidation of $0.0219 \pm 0.0010$ $s^{-1}$ and an apparent $K_d$ of $57 \pm 4$ $\mu$M for $CH_2$-$H_4$folate. (B) Photoreduced enzyme (50 $\mu$M) was mixed with solutions of 50 (○ and ●), 100 (□ and ■), and 300 $\mu$M $CH_2$-$H_4$folate (△ and ▲) (concentrations after mixing). Reaction traces at 430 nm (left axis, filled symbols) and at 337 nm (right axis, empty symbols) are shown. The 337 nm traces have been aligned at a beginning absorbance of 0.22 to more easily visualize them. Reaction conditions were 50 mM potassium phosphate buffer (pH 7.2) containing 0.3 mM EDTA and 10% glycerol at 4 °C.

proposals. To study the oxidative half-reaction, the mutant enzyme was photoreduced and reacted with $CH_2$-$H_4$folate in a stopped-flow spectrophotometer at pH 7.2 and 4 °C. The 450 nm traces for the Asp120Ala mutant are shown in Figure 6A. Indeed, the overall reoxidation of the mutant by $CH_2$-$H_4$folate has been slowed significantly compared to that of the wild-type enzyme. The reaction is triphasic, similar to that of the wild-type enzyme, with fast, medium, and slow phases accounting for <4, 58, and 38%, respectively, of the total absorbance change. The medium phase of the Asp120Ala enzyme was independent of the $CH_2$-$H_4$folate concentration and had an observed rate constant of $0.040 \pm 0.004$ $s^{-1}$ ($k_{med}$, Table 3). By contrast, the slow phase showed a clear hyperbolic dependence on the concentration of $CH_2$-$H_4$folate (inset of Figure 6A). A fit of the data to eq 4 yielded an apparent $K_d$ of $57 \pm 4$ $\mu$M for $CH_2$-$H_4$folate, a significant increase over that observed for the wild-type enzyme at 25 °C. The maximal observed rate constant for the slow phase of reoxidation was $0.0219 \pm 0.0010$ $s^{-1}$, 90-fold lower than the analogous rate constant for the wild-type enzyme (Table 3). These results indicate that both folate binding affinity and rate of catalysis in the oxidative half-reaction have been impaired by the Asp120Ala mutation.

Table 3: Rapid-Reaction Kinetic Constants for the Oxidative Half-Reaction[a]

| | slow phase[b] | | medium phase[c] |
|---|---|---|---|
| enzyme | $K_d$ ($CH_2$-$H_4$folate, $\mu$M) | $k_{slow}$ ($s^{-1}$) | $k_{med}$ ($s^{-1}$)[d] |
| wild type | nd[e] | $1.9 \pm 0.2$[f] | 5.5 |
| Asp120Asn | nd[e] | $0.0077 \pm 0.0002$[f] | 0.022 |
| Asp120Ser | $12 \pm 1$ | $0.0149 \pm 0.0006$[g] | 0.034 |
| Asp120Ala | $57 \pm 4$ | $0.0219 \pm 0.0010$[g] | 0.040 |
| Asp120Val | $108 \pm 21$ | $0.0152 \pm 0.0011$[g] | 0.030 |
| Asp120Lys | $160 \pm 38$ | $0.0105 \pm 0.0009$[g] | 0.040 |

[a] All measurements were taken at 4 °C in 50 mM potassium phosphate buffer (pH 7.2) containing 0.3 mM EDTA and 10% glycerol. [b] Slow phase of reoxidation. [c] Medium phase of reoxidation. [d] Average value, not dependent on the concentration of $CH_2$-$H_4$folate. Uncertainties are ±10% of the $k_{med}$ value. [e] Not able to be determined. [f] Not dependent on the concentration of $CH_2$-$H_4$folate. [g] Dependent on the concentration of $CH_2$-$H_4$folate in a hyperbolic manner.

Stopped-flow studies of the oxidative half-reaction were also carried out with MTHFR variants Asp120Asn, Asp-120Ser, Asp120Val, and Asp120Lys. For each enzyme, the 450 nm reaction traces fit best to three exponential phases. A small increase in absorbance characterized the fast phase. The medium phase was independent of the concentration of $CH_2$-$H_4$folate and yielded observed rate constants 130−250-fold lower than that for the wild-type enzyme ($k_{med}$, Table 3). For mutants Asp120Ser, -Val, and -Lys, the slow phase showed a clear hyperbolic dependence on $CH_2$-$H_4$folate concentration, and fitting of the data to eq 4 yielded the respective apparent dissociation constants and the observed maximal rate constants given in Table 3. By contrast, no apparent dependence on $CH_2$-$H_4$folate concentration was observed for the Asp120Asn variant (Table 3). The results show, within the uncertainty of the measurements, the following trend in apparent $K_d$ values: wild type (Asp 120) ∼ Asn ∼ Ser < Ala < Val ∼ Lys. Moreover, the Asp 120 mutations decrease the rate of folate catalysis 100−300-fold; the Asp120Asn and Asp120Lys enzymes are the most negatively affected.

To test whether the mutant enzymes could form the intermediate species we had observed for the wild-type enzyme at 337 nm, we examined the reaction of the severely impaired Asp120Lys enzyme (50 $\mu$M, after mixing) with $CH_2$-$H_4$folate in the stopped-flow apparatus. No change in absorbance at 337 nm was observed (data not shown). The experiment was then repeated with the more active Asp120Ala mutant. The resulting 337 and 430 nm reaction traces are shown in Figure 6B. At 337 nm, an intermediate species is clearly formed by 2 s and then decays at a rate coincident with flavin reoxidation at 430 nm. At 50−300 $\mu$M $CH_2$-$H_4$-folate, the observed rate constant for the fast phase is estimated to be $2.0 \pm 0.1$ $s^{-1}$. Thus, mutation at the Asp 120 position appears not to prevent formation of the intermediate species, but the rate of its formation is more than 100-fold slower than with the wild-type enzyme.

*The Folate Half-Reaction Is Rate-Limiting for Asp 120 Mutants in the Physiological NADH−$CH_2$-$H_4$Folate Oxidoreductase Reaction.* In the physiological NADH−$CH_2$-$H_4$folate oxidoreductase reaction, NADH transfers reducing

Table 4: Steady-State Kinetic Constants for the NADH−$CH_2$-$H_4$Folate Oxidoreductase Assay[a]

| enzyme | $k_{cat}$ ($s^{-1}$) | $K_m$ (NADH, $\mu$M) | $K_m$ ($CH_2$-$H_4$folate, $\mu$M) | $k_{cat}/K_m$ ($CH_2$-$H_4$folate, $\mu M^{-1}$ $s^{-1}$) |
|---|---|---|---|---|
| wild type[b] | 2.2 ± 0.2 | 3.5 ± 0.6 | 0.40 ± 0.10 | 5.5 |
| Asp120Asn | 0.0073 ± 0.0007 | <3.5 | 17 ± 3 | 0.00043 |
| Asp120Ser | 0.0197 ± 0.0014 | <3.5 | 43 ± 2 | 0.00046 |
| Asp120Ala | 0.0222 ± 0.0020 | <3.5 | 99 ± 7 | 0.00022 |
| Asp120Val | 0.0172 ± 0.0017 | <3.5 | 187 ± 26 | 0.000092 |
| Asp120Lys | 0.0107 ± 0.0014[c] | <3.5 | 142 ± 40[c] | 0.000075 |

[a] All measurements were taken at 4 °C in 50 mM potassium phosphate buffer (pH 7.2) containing 0.3 mM EDTA and 10% glycerol. [b] Wild-type enzyme data were fit to eq 6 for double-substrate inhibition. The $K_i$ for NADH was determined to be 14 ± 6 $\mu$M; the $K_i$ for $CH_2$-$H_4$folate was 61 ± 16 $\mu$M. Mutant enzymes did not exhibit substrate inhibition. [c] Average of two determinations.

equivalents to the enzyme-bound FAD, which in turn transfers them to $CH_2$-$H_4$folate. Steady-state analysis of the physiological reaction was performed under anaerobic conditions in a stopped-flow spectrophotometer at pH 7.2 and 4 °C. With the wild-type enzyme, marked inhibition was observed at high concentrations of each substrate and the kinetic constants were determined by fitting the data to eq 6 by successive iterations. By contrast, the mutant enzymes exhibited no inhibition, and the data were fit to the Michaelis−Menten equation (eq 5). The kinetic parameters obtained for the wild-type and mutant enzymes are shown in Table 4. For the Asp120Asn mutant, $k_{cat}$ was determined to be 0.0073 ± 0.0007 $s^{-1}$, 300-fold lower than that of the wild-type enzyme. This observed turnover number is in good agreement with an expected value of 0.0077 $s^{-1}$ that is calculated from the observed rate constants for the two half-reactions, reduction by NADH ($k_2'$, 20.2 $s^{-1}$, Table 2) and the slow phase of reoxidation by $CH_2$-$H_4$folate ($k_{slow}$, 0.0077 $s^{-1}$, Table 3), assuming a ping-pong bi-bi mechanism (*52*).

$$\frac{v}{[E_t]} = \frac{k_2' k_{slow}}{k_2' + k_{slow}}\ s^{-1} = \frac{(20.6)(0.0077)}{(20.6 + 0.0077)} = 0.0077\ s^{-1} \quad (8)$$

Indeed, the oxidative half-reaction involving $CH_2$-$H_4$folate is rate-limiting in turnover for the Asp120Asn mutant. A similar conclusion can be drawn for the wild-type and other mutant enzymes, given the near equivalence between the maximal turnover numbers ($k_{cat}$) in Table 4 and the maximal observed rate constants obtained from the slow phase of the oxidative half-reaction ($k_{slow}$, Table 3). Our results in Table 4 further show that the mutant enzymes exhibit $K_m$ values for $CH_2$-$H_4$folate increased 50−500-fold compared to that of the wild-type enzyme. $K_m$ values for NADH, however, are smaller in the Asp 120 mutants than in the wild-type enzyme. Such a decrease in $K_m$ for the substrate in the half-reaction that becomes less rate-limiting has been observed previously in enzymes that exhibit ping-pong kinetics (*53*).

## DISCUSSION

*Asp 120 Modulates Flavin Reactivity.* In flavoproteins, the protein environment surrounding the flavin is predicted to have significant influence over the redox properties of the enzyme-bound flavin. Consistent with this view are studies probing the interactions of amino acids with the N5 (*54*−*56*), N3 (*57*), N1 (*58*), and C4 carbonyl (*59*) positions of the flavin isoalloxazine ring in various flavoproteins. In flavoproteins that catalyze dehydrogenase reactions, the N1−C2═O position of the flavin is usually in contact with (within 3.5 Å) a positively charged moiety, either an amino acid (Arg, Lys, or His) or the positive end of a helix dipole (*9*). Most mutagenesis studies carried out to examine how the N1−C2═O moiety controls the redox properties in this class of flavoproteins, however, have been plagued with problems of enzyme inactivity (*15*−*17*), until recently (*60*, *61*). Three roles for the N1−C2═O moiety have been proposed (*9*): (1) assistance in flavin binding, (2) control of flavin midpoint potential, and (3) influence on the protonation state of the reduced hydroquinone (Figure 1B,C).

We have carried out this mutagenesis study to test the importance of the unusual occurrence of a negatively charged residue (Asp 120) near the N1−C2═O moiety of the isoalloxazine moiety in *E. coli* MTHFR (*5*). We have replaced Asp 120 with the following amino acids: Asn, Ser, Ala, Val, and Lys. The fact that the mutant enzymes could be isolated in soluble form with FAD bound (Figure 3) indicates that the N1−C2═O moiety is not required for flavin binding in MTHFR. All midpoint potentials of the mutants (Table 1) were greater than that of the wild-type enzyme (−237 ± 4 mV). From this, we predict that the mutants will be more readily reduced by NADH and, in the reduced form, react less completely with $CH_2$-$H_4$folate than with the wild-type enzyme. Within the uncertainty of the measurements, the mutant midpoint potentials fell into three classes: (1) a 17−19 mV increase in potential for replacement of the negatively charged Asp 120 with the polar, neutral Asn or Ser or the small, nonpolar Ala, (2) a 23 mV increase for substitution with the larger, nonpolar Val, and (3) a 30 mV increase for substitution with Lys. Although the p$K_a$ of the Asp120Lys side chain is not known, the large +30 mV increase in the mutant potential is consistent with a change from a negative charge to a positive charge in the Asp120Lys enzyme. The somewhat similar midpoint potentials of the Asp120Val and Asp120Lys mutants (−214 ± 3 and −207 ± 3 mV, respectively), however, could argue against this supposition. Although the observed changes are not large, our results, taken together, suggest that the midpoint potential of the enzyme-bound FAD in MTHFR is indeed modulated in a manner generally consistent with that expected from the negative charge density of the amino acid at position 120. For comparison, when Lys 266, a positively charged amino acid near the N1−C2═O position of lactate monooxygenase, was replaced with a neutral Met, the midpoint potential was lowered by 31 mV (*10*). In *p*-hydroxybenzoate hydroxylase, where a positive dipole from an α-helix (residues 296−300) is near the N1−C2═O position, a Lys297Met mutation demonstrated a more modest decrease in potential of 13 ± 4 mV (*60*). Similarly, substitution of the N1−C2═O moiety Arg 238 in morphinone reductase with Met resulted in a 12 ± 6 mV lowering of the midpoint potential (*61*). Our 30 ± 3 mV change in potential due to the Asp120Lys mutation in *E. coli* MTHFR stands in contrast, however, to a small 3 ± 4 mV decrease in potential reported for the Arg233Glu mutation in morphinone reductase (*61*). In this last study with morphinone reductase, because the magnitude of their observed changes was small and did not correlate well with the charge of the moiety near the N1−C2═O position, the authors concluded that the

Scheme 3: Kinetic Mechanism for the Oxidative Half-Reaction

$$E_{red} + CH_2\text{-}H_4folate \underset{k_{-4}}{\overset{k_4}{\rightleftharpoons}} E_{red}\bullet CH_2\text{-}H_4folate \underset{k_{-5}}{\overset{k_5}{\rightleftharpoons}} E_{ox}\bullet CH_3\text{-}H_4folate \underset{k_{-6}}{\overset{k_6}{\rightleftharpoons}} E_{ox} + CH_3\text{-}H_4folate$$

charge density near the N1−C2═O position does not contribute significantly to stabilization of the reduced flavin. Similar mutagenesis studies on other flavoproteins are necessary for the full evaluation of the relationship between the N1−C2═O moiety and the midpoint potential of the enzyme-bound FAD. Finally, work is in progress to evaluate the effect of the Asp 120 mutations on the protonation state of the reduced FAD in *E. coli* MTHFR. $^{15}N$ NMR studies on old yellow enzyme (*11*), glucose oxidase (*12*), and flavocytochrome $b_2$ (*13*), flavoproteins that catalyze dehydrogenase reactions and have Arg, His, and Lys, respectively, at the N1−C2═O position, have shown that the reduced flavins in these enzymes are bound as the anionic hydroquinones. Similar studies on N1−C2═O mutant forms of flavin dehydrogenases have not been performed.

*Asp 120 Has a Minor Role in the NADH Half-Reaction.* Mutations that increase the midpoint potential of the flavin are expected to increase the rate of reduction by NADH. Consistent with this view, the rate of enzyme reduction by NADH was increased slightly (1.2−1.5-fold) in the Asp 120 mutants compared to the wild-type enzyme (Table 2). By comparison, a much larger effect (45-fold) on the rate of NADH-linked reduction was observed for the Arg239Met mutant of morphinone reductase (*61*), and for the Lys266Met mutant of lactate monooxygenase, which catalyzed reduction by L-lactate 23000-fold slower than the wild-type enzyme (*10*). As suggested by the authors (*10*, *61*), these large decreases in rates of flavin reduction, however, are likely not due to the altered midpoint potentials of the flavins [decreases of 12 and 31 mV for the mutants of morphinone reductase (*61*) and lactate monooxygenase (*10*), respectively, compared to those of the corresponding wild-type enzymes] and may, rather, reflect altered substrate binding or reaction intermediate stabilization in the mutant enzymes.

*A Proposed Mechanism for the Folate Half-Reaction.* From Scheme 1, a four-step sequence of events can be envisioned for the $CH_2$-$H_4$folate oxidative half-reaction: (1) binding of $CH_2$-$H_4$folate to the reduced enzyme to form a Michaelis complex, perhaps coupled to the enforcing of the proper orientation of the substrate for catalysis, as proposed for thymidylate synthase (*20*, *62*, *63*), (2) protonation of N10 by an acid catalyst to promote opening of the imidazolidine ring and formation of the 5-iminium cation, (3) transfer of a hydride from the reduced FAD to a stabilized 5-iminium cation, and (4) release of the product $CH_3$-$H_4$folate.

Taken together, our results for the wild-type enzyme may be described by the minimal kinetic mechanism for the oxidative half-reaction, shown as Scheme 3. When the reduced wild-type enzyme is reacted with $CH_2$-$H_4$folate in the stopped-flow spectrophotometer, the reaction traces at 450 and 337 nm are triphasic (Figure 5). The small, fast phase at 450 nm represents an initial lag in the reaction corresponding to the formation of a reduced enzyme−folate complex at 337 nm, which is independent of the concentration of $CH_2$-$H_4$folate. The medium and slow phases, also independent of $CH_2$-$H_4$folate concentration, show decay of this complex at 337 nm, concomitant with flavin reoxidation at 450 nm (Figure 5B). To test whether the complex could be the $E_{red}$•5-iminium cation species, we performed a secondary isotope effect experiment using $CD_2$-$H_4$folate in place of $CH_2$-$H_4$folate in the oxidative half-reaction. Our failure, however, to see a secondary isotope effect (data not shown) is not consistent with the 337 nm species being the 5-iminium cation. Our results stand in contrast to recent kinetic data obtained at 337 nm in support of a 5-iminium cation in the reaction of thymidylate synthase with $CH_2$-$H_4$-folate (*64*). An $E_{red}$•$CH_2$-$H_4$folate complex would also be consistent with the observed perturbation of the spectrum of the reduced enzyme. Thus, we hypothesize that the intermediate species observed at 337 nm is either the initial $E_{red}$•$CH_2$-$H_4$folate Michaelis complex as depicted in Scheme 3 or, possibly, a strained, bent conformation in which the $CH_2$-$H_4$folate is better oriented for catalysis, as suggested for thymidylate synthase (*20*, *62*, *63*).

The medium and slow phases of the oxidative half-reaction account for 68 and 28%, respectively, of the observed absorbance increase at 450 nm and show no dependence on the concentration of $CH_2$-$H_4$folate. Two phases of oxidation were also observed in our earlier study with the wild-type enzyme at 25 °C (*4*). Flavin oxidation is also clearly reversible, as indicated by the failure of the oxidative half-reaction to go to completion except at high (100−200 $\mu$M) concentrations of $CH_2$-$H_4$folate (Figure 5). [The free energy change of the half-reaction is calculated to be −1.2 kcal/mol (*4*).] Two mechanisms can be proposed to account for the biphasic kinetics of the folate half-reaction. The first, suggested by one of our referees, proposes that the slow and medium phases correspond to the reversible oxidation and product release steps, respectively, in Scheme 3. A second possible mechanism is that the two phases are somehow both involved in flavin reoxidation and that the $CH_3$-$H_4$folate product release step is very fast in comparison. In this case, we speculate that the medium and slow phases could represent two populations of enzyme, perhaps differing by subunit asymmetry or conformational change, that reoxidize at two different rates. The observed rate constants for the oxidative half-reaction and for overall catalysis are given by eqs 9 and 10, respectively.

$$k_5' = \frac{k_5 k_6}{k_{-5} + k_6} \tag{9}$$

$$k_{cat} = \frac{k_5 k_6}{k_5 + k_{-5} + k_6} \tag{10}$$

In support of the second mechanism, the net rate constant for the slow phase measured in the stopped-flow instrument, $k_5'$ ($k_{slow}$ of 1.9 ± 0.2 $s^{-1}$, Table 3), is nearly the same as $k_{cat}$ (2.2 ± 0.2 $s^{-1}$, Table 4). From eqs 9 and 10, this equivalence implies that $k_5 \ll k_{-5} + k_6$, which will be the case if $k_6 \gg k_5$; i.e., $CH_3$-$H_4$folate product release is at least 10-fold faster than flavin oxidation. Thus, a 5.5 ± 0.6 $s^{-1}$ value for the observed rate constant of the medium phase should not qualify for $k_6$. To try to determine a reasonable value for $k_6$, we have attempted simulations of the folate half-reaction at 450/430 and 337 nm using an A + B ↔ C ↔ D ↔ E + F model and 10−600 $\mu$M $CH_2$-$H_4$folate. The following rate constants (assignments according to Scheme 3) give reasonable fits to our experimental data at 430 nm, with 50 $\mu$M

enzyme: $k_4 = 1 \times 10^6$ $M^{-1}$ $s^{-1}$, $k_{-4} = 15$ $s^{-1}$, $k_5 = 3$ $s^{-1}$, $k_{-5} = 2$ $s^{-1}$, $k_6 = 30$ $s^{-1}$, and $k_{-6} = 6 \times 10^6$ $M^{-1}$ $s^{-1}$ (available as Supporting Information). Using these rate constants, the net rate constant for the slow phase of the oxidative-half reaction, $k_5'$, is calculated from eq 9 to be 2.7 $s^{-1}$ and the $k_{cat}$ is calculated from eq 10 to be 2.4 $s^{-1}$, values somewhat higher than the experimental ones, $1.9 \pm 0.2$ and $2.2 \pm 0.2$ $s^{-1}$, respectively. Essentially the same fits, however, are obtained by lowering $k_6$ to 5.5 $s^{-1}$ and $k_{-6}$ to $1 \times 10^6$ $M^{-1}$ $s^{-1}$, which result in calculated values of 2.2 and 1.6 $s^{-1}$ for $k_5'$ and $k_{cat}$, respectively (see the Supporting Information). Because the simulations show that a value for $k_6$ of 30 or 5.5 $s^{-1}$ can accommodate the data, we cannot, at this time, confidently distinguish between our two proposed mechanisms cited above. Further experiments are necessary. Note that the Asp 120 mutants, investigated in this work, also show the two phases of oxidation.

*Asp 120 Has a Major Role in Folate Binding.* Modeling of the $CH_3$-$H_4$folate product into the enzyme active site (Figure 2) suggested a role for Asp 120 in the binding of $CH_2$-$H_4$folate (step 1 in Scheme 3). In the model, which has been confirmed recently by the structure of an enzyme−$CH_3$-$H_4$folate complex (R. Pejchal and M. L. Ludwig, personal communication), the carboxylate oxygens of Asp 120 form bidentate hydrogen bonds with the N3 and 2-amino groups of the pterin ring. To investigate the role of Asp 120 in folate binding, we examined the affinity of mutants Asp120Asn, -Ser, -Ala, -Val, and -Lys for $CH_2$-$H_4$folate during the oxidative half-reaction at 4 °C. Rate constant data (from the slow phase) for mutants Asp120Ser, -Ala, -Val, and -Lys were fit to hyperbolic eq 4 to obtain apparent $K_d$ values for $CH_2$-$H_4$folate (Table 3). A hyperbolic dependence on $CH_2$-$H_4$folate was not observed for wild-type and Asp120Asn MTHFR (Table 3), as had been seen for these enzymes in our previous studies at 25 °C (*4*, *18*). In comparison to the apparent $K_d$ of the wild-type enzyme measured at 25 °C ($11 \pm 1$ $\mu$M) (*4*), increases in affinity from 1.4- to 15-fold were observed for mutants Asp120Ser, -Ala, -Val, and -Lys (Table 3). The Asp120Asn mutant demonstrated an apparent $K_d$ of $21 \pm 3$ $\mu$M at 25 °C (*18*). Our combined results at 25 and 4 °C indicate that, indeed, Asp 120 significantly participates in folate binding, a result consistent with findings for analogous aspartates in the folate-dependent enzymes dihydrofolate reductase (*65*), thymidylate synthase (*66*), and bifunctional methylenetetrahydrofolate dehydrogenase-cyclohydrolase (*67*). Moreover, the observed trend in apparent $K_d$ values (wild type ∼ Asn ∼ Ser < Ala < Val ∼ Lys) may be explained in terms of the weakening ability of the mutant side chains to hydrogen bond to the pterin ring of the folate molecule. In particular, compared to the wild-type enzyme [apparent $K_d$ of $11 \pm 1$ $\mu$M at 25 °C (*4*)], the Asp120Asn and -Ser variants, which could retain hydrogen bonding to the pterin ring, reduce the affinity for $CH_2$-$H_4$folate minimally (∼2-fold); the small Asp120Ala enzyme, perhaps with the aid of an appropriately positioned water molecule hydrogen bonded to the pterin, decreases the affinity slightly more (5-fold), and the larger Asp120Val variant, which presumably has no hydrogen bonding ability and may cause steric interference, reduces affinity 11-fold. Finally, a large decrease in the extent of folate binding (15-fold) for the Asp120Lys mutant similar to that for the Val mutant suggests an influence from sterics in positioning of the Lys side chain; the Lys side chain may be pointed away from the pterin ring to avoid a steric clash and not in a position for the NH-containing side chain to hydrogen bond to the folate. To support such speculations, structural characterization of mutant−folate complexes is necessary, and these studies are planned as future work.

*Asp 120 Has a Major Role in $CH_2$-$H_4$Folate Catalysis.* From our $CH_3$-$H_4$folate docking model (Figure 2), we hypothesized a role for Asp 120 in folate catalysis, perhaps in electrostatic stabilization of the putative 5-iminium cation intermediate. The negatively charged carboxylate side chain of Asp 120, hydrogen bonded to the N3 and 2-amino groups of the pterin ring and located an estimated 6.3 Å from the N5 atom of the pterin ring, could have favorable long-range electrostatic interactions with a positively charged 5-iminium cation. Similar long-range interactions have been proposed to explain the role of Asp 27 of dihydrofolate reductase in elevating the p$K_a$ of the N5 atom of dihydrofolate (*68*). In this study, the Asp 120 mutants showed a 100−300-fold decreased rate in the oxidative half-reaction involving $CH_2$-$H_4$folate (both slow and medium phases, Table 3) and in the steady-state NADH−$CH_2$-$H_4$folate oxidoreductase assay (Table 4), where the folate half-reaction was rate-limiting, thereby showing the importance of Asp 120 in catalysis. Within the error of the measurements, catalytic efficiency ($k_{cat}/K_m$) in the physiological oxidoreductase reaction varied in the following order: wild type ≫ Asn ∼ Ser > Ala > Val ∼ Lys (Table 4). Replacement of the negatively charged Asp 120 with a polar, neutral Asn or Ser led to a 12000-fold decrease in $k_{cat}/K_m$, while the small, nonpolar Asp120Ala mutant, perhaps in combination with an intermediary water molecule, exhibited a 25000-fold decrease. Of the mutants, the most significantly impaired (by 70000-fold) were the large, nonpolar Val and the large and, presumably, positively charged Lys. Taken together, these data suggest a general correlation between catalytic efficiency and the negative charge density at position 120, a finding consistent with a role for Asp 120 in electrostatic stabilization of the putative 5-iminium cation intermediate during catalysis.

Our results indicate that Asp 120 functions in the binding and reduction of $CH_2$-$H_4$folate. On the basis our stopped-flow data at 337 nm, we speculate further that Asp 120 may be involved in enforcing or binding to a catalytically competent conformation of $CH_2$-$H_4$folate, as proposed for the analogous Asp 169 in thymidylate synthase (*62*, *63*). In our studies, a pre-steady-state species was detected at 337 nm for the wild-type enzyme (Figure 5B) and for the most active Asp120Ala mutant (Figure 6B), but not for the most severely impaired Asp120Lys mutant (data not shown). In addition, the formation of the complex in the Asp120Ala mutant, possibly aided by the hydrogen bonding of an intermediary water molecule to the pterin, was slowed almost 300-fold in Asp120Ala compared to the wild-type enzyme. Taken together, these results suggest that while Asp 120 is not essential for formation of the complex, it aids significantly in its formation, probably via hydrogen bonding interactions with the pterin ring. Furthermore, these results show that the presence of the complex leads to a higher degree of catalytic competency in the Asp 120 mutant enzymes.

In this paper, we have characterized the kinetic and thermodynamic properties of five mutants of *E. coli* MTH-

FR: Asp120Asn, Asp120Ser, Asp120Ala, Asp120Val, and Asp120Lys. Our results establish a major role for Asp 120 in folate binding. Moreover, our finding that catalytic efficiency is reduced in concert with the loss of negative charge density at position 120 is consistent with a role for Asp 120 in electrostatic stabilization of the 5-iminium cation intermediate during catalysis.

## ACKNOWLEDGMENT

We thank Vincent Massey (The University of Michigan) for the gift of 3,10-dimethyl-5-deazaisoalloxazine and Eprova (Schaffhausen, Switzerland) for (6*S*)-$H_4$folate. We acknowledge Grinnell College for generous start-up funds and Emily Burke for help in the setup of the anaerobic train. We thank Martha Ludwig, Rowena Matthews, Robert Pejchal, Bruce Palfey, and L. David Arscott for helpful discussions.

## SUPPORTING INFORMATION AVAILABLE

Methods describing the simulations of the reductive and oxidative half-reactions and plots of the simulated traces. This material is available free of charge via the Internet at http://pubs.acs.org.

## REFERENCES

1. Refsum, H., Ueland, P. M., Nygard, O., and Vollset, S. E. (1998) Homocysteine and Cardiovascular Disease, *Annu. Rev. Med. 49*, 31−62.
2. Shields, D. C., Kirke, P. N., Mills, J. L., Ramsbottom, D., Malloy, A. M., Burke, H., Weir, D. G., Scott, J. M., and Whitehead, A. S. (1999) The "thermolabile" variant of methylenetetrahydrofolate reductase and neural tube defects: An evaluation of genetic risk and the relative importance of the genotypes of the embryo and the mother, *Am. J. Hum. Genet. 64*, 1045−1055.
3. Vanoni, M. A., Ballou, D. P., and Matthews, R. G. (1983) Methylenetetrahydrofolate reductase: Steady state and rapid reaction studies on the NADPH-methylenetetrahydrofolate, NADPH-menadione, and methyltetrahydrofolate-menadione oxidoreductase activities of the enzyme, *J. Biol. Chem. 258*, 11510−11514.
4. Trimmer, E. E., Ballou, D. P., and Matthews, R. G. (2001) Methylenetetrahydrofolate reductase from *Escherichia coli*: Elucidation of the kinetic mechanism by steady-state and rapid-reaction studies, *Biochemistry 40*, 6205−6215.
5. Guenther, B. D., Sheppard, C. A., Tran, P., Rozen, R., Matthews, R. G., and Ludwig, M. L. (1999) The structure and properties of methylenetetrahydrofolate reductase from *Escherichia coli* suggest how folate ameliorates human hyperhomocysteinemia, *Nat. Struct. Biol. 6*, 359−365.
6. Daubner, S. C., and Matthews, R. G. (1982) Purification and properties of methylene-tetrahydrofolate reductase from pig liver, *J. Biol. Chem. 257*, 140−145.
7. Vanoni, M. A., and Matthews, R. G. (1984) Kinetic isotope effects on the oxidation of reduced nicotinamide adenine dinucleotide phosphate by the flavoprotein methylenetetra-hydrofolate reductase, *Biochemistry 23*, 5272−5279.
8. Sumner, J. S., and Matthews, R. G. (1992) Stereochemistry and mechanism of hydrogen transfer between NADPH and methylenetetrahydrofolate in the reaction catalyzed by methylenetetrahydrofolate reductase from pig liver, *J. Am. Chem. Soc. 114*, 6949−6956.
9. Fraaije, M. W., and Mattevi, A. (2000) Flavoenzymes: Diverse catalysts with recurrent features, *Trends Biochem. Sci. 25*, 126−132.
10. Müh, U., Massey, V., and Williams, C. H., Jr. (1994) Lactate monooxygenase. I. Expression of the mycobacterial gene in *Escherichia coli* and site-directed mutagenesis of lysine 266, *J. Biol. Chem. 269*, 7982−7988.
11. Beinert, W.-D., Rüterjans, H., and Müller, F. (1985) Nuclear magnetic resonance studies of the old yellow enzyme. 1. $^{15}$N NMR of the enzyme recombined with $^{15}$N-labeled flavin mononucleotides, *Eur. J. Biochem. 152*, 573−579.
12. Sanner, C., Macheroux, P., Rüterjans, H., Müller, F., and Bacher, A. (1991) $^{15}$N- and $^{13}$C-NMR investigations of glucose oxidase from *Aspergillus niger*, *Eur. J. Biochem. 196*, 663−672.
13. Rüterjans, H., Fleischmann, G., Knauf, M., Lohr, F., Blümel, M., Lederer, F., Mayhew, S. G., and Müller, F. (1996) NMR studies of flavoproteins, *Biochem. Soc. Trans. 24*, 116−121.
14. Ghisla, S., and Massey, V. (1986) New flavins for old: Artificial flavins as active site probes of flavoproteins, *Biochem. J. 239*, 1−12.
15. Bjornberg, O., Rowland, P., Larsen, S., and Jensen, K. F. (1997) Active site dihydroorotate dehydrogenase A from *Lactococcus lactis* investigated by chemical modification and mutagenesis, *Biochemistry 36*, 16197−16205.
16. Mewies, M., Packman, L. C., Mathews, F. S., and Scrutton, N. S. (1996) Flavinylation in wild-type trimethylamine dehydrogenase and differentially charged mutant enzymes: A study of the protein environment around the N1 of the flavin isoalloxazine, *Biochem. J. 317*, 267−272.
17. Reid, G. A., White, S., Black, M. T., Lederer, F., Mathews, F. S., and Chapman, S. K. (1988) Probing the active site of flavocytochrome $b_2$ by site-directed mutagenesis, *Eur. J. Biochem. 178*, 329−333.
18. Trimmer, E. E., Ballou, D. P., Ludwig, M. L., and Matthews, R. G. (2001) Folate activation and catalysis in methylenetetrahydrofolate reductase from *Escherichia coli*: Roles for aspartate 120 and glutamate 28, *Biochemistry 40*, 6216−6226.
19. Carreras, C. W., and Santi, D. V. (1995) The catalytic mechanism and structure of thymidylate synthase, *Annu. Rev. Biochem. 64*, 721−762.
20. Matthews, D. A., Villafranca, J. E., Janson, C. A., Smith, W. W., Welsh, K., and Freer, S. (1990) Stereochemical mechanism of action for thymidylate synthase based on the X-ray structure of the covalent inhibitory ternary complex with 5-fluoro-2′-deoxyuridylate and 5,10-methylenetetrahydrofolate, *J. Mol. Biol. 214*, 937−948.
21. Perry, K. M., Carreras, C. W., Chang, L. C., Santi, D. V., and Stroud, R. M. (1993) Structures of thymidylate synthase with a C-terminal deletion: Role of the C-terminus in alignment of 2′-deoxyuridine 5′-monophosphate and 5,10-methylenetetrahydrofolate, *Biochemistry 32*, 7116−7125.
22. Matthews, D. A., Alden, R. A., Bolin, J. T., Freer, S. T., Hamlin, R., Xuong, N., Kraut, J., Poe, M., Williams, M., and Hoogsteen, K. (1977) Dihydrofolate reductase: X-ray structure of the binary complex with methotrexate, *Science 197*, 452−455.
23. Klein, C., Chen, P., Arevalo, J. H., Stura, E. A., Marolewski, A., Warren, M. S., Benkovic, S. J., and Wilson, I. A. (1995) Towards structure-based drug design: Crystal structure of a multisubstrate adduct complex of glycinamide ribonucleotide transformylase at 1.96 Å resolution, *J. Mol. Biol. 249*, 153−175.
24. Hampele, I. C., D'Arcy, A., Dale, G. E., Kostrewa, D., Nielsen, J., Oefner, C., Page, M. G. P., Schoenfeld, H.-J., Stueber, D., and Then, R. L. (1997) Structure and function of the dihydropteroate synthase from *Staphylococcus aureus*, *J. Mol. Biol. 268*, 21−30.
25. Achari, A., Somers, D. O., Champness, J. N., Bryant, P. K., Rosemond, J., and Stammers, D. K. (1997) Crystal structure of the anti-bacterial sulfonamide drug target dihydropteroate synthase, *Nat. Struct. Biol. 4*, 490−497.
26. Baca, A. M., Sirawaraporn, R., Turley, S., Sirawaraporn, W., and Hol, W. G. (2000) Crystal structure of *Mycobacterium tuberculosis* 7,8-dihydropteroate synthase in complex with pterin monophosphate: New insight into the enzymatic mechanism and sulfa-drug action, *J. Mol. Biol. 302*, 1193−1212.
27. Schmidt, A., Wu, H., MacKenzie, R. E., Chen, V. J., Bewly, J. R., Ray, J. E., Toth, J. E., and Cygler, M. (2000) Structures of three inhibitor complexes provide insight into the reaction mechanism of the human methylenetetrahydrofolate dehydrogenase/cyclohydrolase, *Biochemistry 39*, 6325−6335.
28. Doukov, T., Seravalli, J., Stezowski, J. J., and Ragsdale, S. W. (2000) Crystal structure of a methyltetrahydrofolate- and corrinoid-dependent methyltransferase, *Struct. Folding Des. 8*, 817−830.
29. Wolan, D. W., Greasley, S. E., Wall, M. J., Benkovic, S. J., and Wilson, I. A. (2003) Structure of Avian AICAR transformylase with a multisubstrate adduct inhibitor $\beta$-DADF identifies the folate binding site, *Biochemistry 42*, 10904−10914.
30. Evans, J. C., Huddler, D. P., Hilgers, M. T., Romanchuk, G., Matthews, R. G., and Ludwig, M. L. (2004) Structures of the N-terminal modules imply large domain motions during catalysis by methionine synthase, *Proc. Natl. Acad. Sci. U.S.A. 101*, 3729−3736.

31. Scarsdale, J. N., Radaev, S., Kazanina, G., Schirch, V., and Wright, H. T. (2000) Crystal structure at 2.4 Å resolution of *E. coli* serine hydroxymethyltransferase in complex with glycine substrate and 5-formyl tetrahydrofolate, *J. Mol. Biol. 296*, 155−168.
32. Szebenyi, D. M., Liu, X., Kriksunov, I. A., Stover, P. J., and Thiel, D. J. (2000) Structure of a murine cytoplasmic serine hydroxymethyltransferase quinonoid ternary complex: Evidence for asymmetric obligate dimers, *Biochemistry 39*, 13313−13323.
33. Trivedi, V., Gupta, A., Venkatakrishna, R. J., Saravanan, P., Rao, G. S. J., Rao, N. A., Savithri, H. S., and Subramanya, H. S. (2002) Crystal structure of binary and ternary complexes of serine hydromethyltransferase from *Bacillus stearothermophilus*: Insights into the catalytic mechanism, *J. Biol. Chem. 277*, 17161−17169.
34. Bull, C., and Ballou, D. P. (1981) Purification and properties of protocatechuate 3,4-dioxygenase from *Pseudomonas putida*. A new iron to subunit stoichiometry, *J. Biol. Chem. 256*, 12673−12680.
35. Fasman, G. D. (1976) *Handbook of Biochemistry and Molecular Biology*, 3rd ed., Vol. I, CRC Press, Inc., Cleveland, OH.
36. Blakley, R. L. (1969) *The Biochemistry of Folic Acid and Related Pteridines*, North-Holland, Amsterdam.
37. Horton, R. M., Ho, S. N., Pullen, J. K., Hunt, H. D., Cai, Z., and Pease, L. R. (1993) Gene splicing by overlap extension, *Methods Enzymol. 217*, 270−279.
38. Sheppard, C. A., Trimmer, E. E., and Matthews, R. G. (1999) Purification and properties of NADH-dependent 5,10-methylenetetrahydrofolate reductase (MetF) from *Escherichia coli*, *J. Bacteriol. 181*, 718−725.
39. Whitfield, C. D., Steers, E. J., and Weissbach, H. (1970) Purification and Properties of 5-Methyltetrahydropteroyltriglutamate-Homocysteine Transmethylase, *J. Biol. Chem. 245*, 390−401.
40. Beinert, H. (1960) Flavin coenzymes, in *The Enzymes* (Boyer, P. D., Lardy, H., and Myrback, K., Eds.) pp 339−416, Academic Press, New York.
41. Massey, V. (1991) A simple method for the determination of redox potentials, in *Flavins and Flavoproteins* (Curti, B., Ronchi, S., and Zanetti, G., Eds.) pp 59−66, Walter de Gruyter & Co., Berlin.
42. Clark, W. M. (1960) *Oxidation−Reduction Potentials of Organic Systems*, Williams & Wilkens Co., Baltimore.
43. Minnaert, K. (1965) Measurement of the equilibrium constant of the reaction between cytochrome *c* and cytochrome *a*, *Biochim. Biophys. Acta 110*, 42−56.
44. Patil, P. V., and Ballou, D. P. (2000) The use of protocatechuate dioxygenase for maintaining anaerobic conditions in biochemical experiments, *Anal. Biochem. 286*, 187−192.
45. Massey, V., and Hemmerich, P. (1978) Photoreduction of flavoproteins and other biological compounds catalyzed by deazaflavins, *Biochemistry 17*, 9−17.
46. Press, W. H., Teulosky, S. A., Vettering, W. T., and Flannery, B. P. (1992) *Numerical methods in C*, 2nd ed., Cambridge University Press, Cambridge, U.K.
47. Kutzbach, C., and Stokstad, E. L. R. (1971) Mammalian methylenetetrahydrofolate reductase: Partial purification, properties, and inhibition by *S*-adenosylmethionine, *Biochim. Biophys. Acta 250*, 459−477.
48. Matthews, R. G. (1986) Methylenetetrahydrofolate reductase from pig liver, *Methods Enzymol. 122*, 372−381.
49. Cleland, W. W. (1979) Substrate Inhibition, *Methods Enzymol. 63*, 500−513.
50. Cleland, W. W. (1975) Partition analysis and the concept of net rate constants as tools in enzyme kinetics, *Biochemistry 14*, 3220−3224.
51. Bruice, T. W., Garrett, C., Wataya, Y., and Santi, D. V. (1980) Use of secondary α-hydrogen isotope effects in reactions of pyrimidine nucleoside/nucleotide metabolism: Thymidylate synthase, *Methods Enzymol. 64*, 125−135.
52. Massey, V., Gibson, Q. H., and Veeger, C. (1960) Intermediates in the catalytic action of lipoyl dehydrogenase (diaphorase), *Biochem. J. 77*, 341−351.
53. Matthews, R. G. (1990) $K_m$ effects associated with site-directed mutations that reduce the velocity of one half reaction of a ping pong mechanism, in *Flavins and Flavoproteins* (Curti, B., Ronchi, S., and Zanetti, G., Eds.) Walter de Gruyter & Co., Berlin.
54. Ludwig, M. L., Pattridge, K. A., Metzger, A. L., and Dixon, M. M. (1997) Control of oxidation−reduction potentials in flavodoxin from *Clostridium beijerinckii*: The role of conformational changes, *Biochemistry 36*, 1259−1280.
55. O'Farrell, P. A., Walsh, M. A., McCarthy, A. A., Higgins, T. M., Voordouw, G., and Mayhew, S. G. (1998) Modulation of the redox potentials of FMN in *Desulfovibrio vulgaris* flavodoxin: Thermodynamic properties and crystal structures of glycine-61 mutants, *Biochemistry 37*, 8405−8416.
56. Chang, F.-C., and Swenson, R. P. (1999) The midpoint potentials for the oxidized-semiquinone couple for Gly57 mutants of the *Clostridium beijerinckii* flavodoxin correlate with changes in the hydrogen-bonding interaction with the proton on N(5) of the reduced flavin mononucleotide cofactor as measured by NMR chemical shift temperature dependencies, *Biochemistry 38*, 7168−7176.
57. Bradley, L. H., and Swenson, R. P. (1999) Role of glutamate-59 hydrogen bonded to $N_3H$ of the flavin mononucleotide cofactor in the modulation of the redox potentials of *Clostridium beijerinckii* flavodoxin: Glutamate-59 is not responsible for the pH dependency but contributes to the stabilization of the flavin semiquinone, *Biochemistry 38*, 12377−12386.
58. Geoghegan, S. M., Mayhew, S. G., Yalloway, G. N., and Butler, G. (2000) Cloning, sequencing and expression of the gene for flavodoxin from *Megasphaera elsdenii* and the effects of removing the protein negative charge that is closest to N(1) of the bound FMN, *Eur. J. Biochem. 267*, 4434−4444.
59. Xu, D., Kohli, R. M., and Massey, V. (1999) The role of threonine 37 in flavin reactivity of the old yellow enzyme, *Proc. Natl. Acad. Sci. U.S.A. 96*, 3556−3561.
60. Ortiz-Maldonado, M., Aeschliman, S. M., Ballou, D. P., and Massey, V. (2001) Synergistic interactions of multiple mutations on catalysis during the hydroxylation reaction of *p*-hydroxybenzoate hydroxylase: Studies of the Lys297Met, Asn300Asp, and Tyr385Phe mutants reconstituted with 8-Cl-Flavin, *Biochemistry 40*, 8705−8716.
61. Craig, D. H., Barna, T., Moody, P. C. E., Bruce, N. C., Chapman, S. K., Munro, A. W., and Scrutton, N. S. (2001) Effects of environment on flavin reactivity in morphinone reductase: Analysis of enzymes displaying differential charge near the N-1 atom and C-2 carbonyl region of the active-site flavin, *Biochem. J. 359*, 315−323.
62. Sage, C. R., Michelitsch, M. D., Stout, T. J., Biermann, D., Nissen, R., Finer-Moore, J., and Stroud, R. M. (1998) D221 in thymidylate synthase controls conformation change, and thereby opening of the imidazolidine, *Biochemistry 37*, 13893−13901.
63. Birdsall, D. L., Finer-Moore, J., and Stroud, R. M. (2003) The only active mutant of thymidylate synthase D169, a residue far from the site of methyl transfer, demonstrates the exquisite nature of enzyme specificity, *Protein Eng. 16*, 229−240.
64. Johnson, E. F., Hinz, W., Atreya, C. E., Maley, F., and Anderson, K. S. (2002) Mechanistic characterization of *Toxoplasma gondii* thymidylate synthase (TS-DHFR)-dihydrofolate reductase: Evidence for a TS intermediate and TS half sites reactivity, *J. Biol. Chem. 277*, 43126−43136.
65. Howell, E. E., Villafranca, J. E., Warren, M. S., Oatley, S. J., and Kraut, J. (1986) Functional role of aspartic acid-27 in dihydrofolate reductase revealed by mutagenesis, *Science 231*, 1123−1128.
66. Chiericatti, G., and Santi, D. V. (1998) Aspartate 221 of thymidylate synthase is involved in folate cofactor binding and in catalysis, *Biochemistry 37*, 9038−9042.
67. Sundararajan, S., and MacKenzie, R. E. (2002) Residues involved in the mechanism of the bifunctional methylenetetrahydrofolate dehydrogenase-cyclohydrolase: The role of glutamine 100 and aspartate 125, *J. Biol. Chem. 277*, 18703−18709.
68. Chen, Y.-Q., Kraut, J., Blakley, R. L., and Callender, R. (1994) Determination by Raman spectroscopy of the $pK_a$ of N5 of dihydrofolate bound to dihydrofolate reductase: Mechanistic implications, *Biochemistry 33*, 7021−7026.
69. Franken, H.-D., Rüterjans, H., and Müller, F. (1984) Nuclear-magnetic-resonance investigation of $^{15}N$-labeled flavins, free and bound to *Megashaera elsdenii* apoflavodoxin, *Eur. J. Biochem. 138*, 481−489.
70. Lee, H., Reyes, V. M., and Kraut, J. (1996) Crystal structures of *Escherichia coli* dihydrofolate reductase complexed with 5-formyltetrahydrofolate (folinic acid) in two space groups: Evidence for enolization of pteridine O4, *Biochemistry 35*, 7012−7020.


BI0477236